A new species of mesonychian mammal from the lower Eocene of Mongolia and its phylogenetic relationships

JONATHAN H. GEISLER and MALCOLM C. MCKENNA

We describe *Dissacus zanabazari* new species from a partial skeleton collected from the early Eocene Bumban Member of the Naran Bulak Formation at Tsagaan Khushuu (Omnogov Province, Mongolia). The holotype includes most of the skull with basicranium, mandibles, well preserved upper and lower dentitions, partially articulated left manus and right tarsus, and most of the long bones in the limbs. The presence of a rudimentary 1st metatarsal is confirmed in mesonychids, and the relatively unworn lower incisors display an unexpected trilobed morphology. Autapomorphies of this new species are short face, absence of diastemata between the lower premolars (except between p1 and p2), m3 metaconid subequal to protoconid, and foramen for superior ramus of stapedial artery entirely within the petrosal. A phylogenetic analysis of 89 characters scored for 14 mesonychians and 5 outgroups resulted in 8 most parsimonious trees. *Dissacus zanabazari* is in a clade with *D. navajovius*, but this genus is otherwise paraphyletic. The strict consensus of the eight trees has a monophyletic Mesonychia, Hapalodectidae, and Mesonychidae; *Dissacus* and *Ankalagon* as the most basal mesonychid genera; and paraphyly of *Pachyaena*.

Key words: Mammalia, Mesonychia, Mesonychidae, *Dissacus*, Eocene, Bumbanian, Tsagan Khushuu, Mongolia.

Jonathan H. Geisler [geislerj@georgiasouthern.edu], Department of Geology and Geography and Georgia Southern Museum, Georgia Southern University, Statesboro, GA 30460, and Research Associate, Division of Paleontology, American Museum of Natural History;
Malcolm C. McKenna [m4pmck@indra.com], Curator Emeritus, Division of Paleontology, American Museum of Natural History, and Adjunct Professor, Department of Geology and Geophysics, University of Wyoming, Laramie, WY 82071.

Introduction

In August of 1997, the MAE (Mongolian Academy of Sciences and American Museum of Natural History joint expedition) visited exposures of the Naran Bulak Formation at Tsagaan Khushuu, located in Omnogov Province, Mongolia. During the first day of prospecting, the second author (M.C. McKenna) discovered a partial skeleton, including a nearly complete skull, of a new species of *Dissacus* from the Bumban Member of the Naran Bulak Formation. Although fossils of *Dissacus indigenus* have been found in the underlying Naran Member of the Naran Bulak Formation (Dashzeveg 1976), this genus had not been reported from the Bumban Member. In fact, nearly all other fossils found from the same stratigraphic level as our new species of *Dissacus* have been referred to *Rhombomylus* (Dashzeveg and Russell 1988) or *Gomphos* (Asher et al. 2005), two genera of gliriform mammals.

Dissacus Cope, 1881 is the most basal genus within Mesonychidae (Zhou et al. 1995; O'Leary 1998a; Geisler and Uhen 2003) and includes some of the oldest species within this family (O'Leary and Rose 1995a). This genus achieved a Holarctic distribution in the late Paleocene (McKenna and Bell 1997), with four named species in Asia: *Dissacus rotundus* Wang, 1975, *D. indigenus* Dashzeveg,

1976, *D. magushanensis* Yan and Tang, 1976, *D. serratus* Chow and Qi, 1978 (Meng et al. 1988), and *D. zengi* Ting, Wang, Schiebout, Koch, Clyde, Bowen, and Wang, 2004, *D. europaeus* Lemoine, 1891 being the only valid species in Europe; and three or four valid species in North America (O'Leary and Rose 1995a). Two and possibly three species of *Dissacus* are known from the early Eocene of North America (O'Leary and Rose 1995a), and undescribed material has been reported from the early Eocene Wutu fauna of China (Tong and Wang 1988). Prior to this report, *Dissacus* was known only by dentitions, fragmentary cranial material, and a few postcranial elements (e.g., Cope 1881; O'Leary and Rose 1995a). Thus the new material sheds considerable light on the morphology of this genus as well as the primitive morphology of Mesonychidae.

Until recently, Mesonychidae was widely thought to be closely related to Cetacea, either as its exclusive sister-group (Geisler and Luo 1998), or together with Hapalodectidae as its sister-group (O'Leary 1998a), or to be a paraphyletic grade from which Cetacea arose (Van Valen 1966; Geisler 2001). The discovery of well preserved hind limbs of archaic cetaceans (Gingerich et al. 2001; Thewissen et al. 2001) and later phylogenetic analyses that incorporated these findings (Geisler and Uhen 2003; 2005; Boisserie et al. 2005) have

Acta Palaeontol. Pol. 52 (1): 189–212, 2007

http://app.pan.pl/acta52/app52-189.pdf

shown that cetaceans are more closely related to hippo-potamids and other artiodactyls than they are to mesony-chids, a result consistent with many molecular studies (e.g. Gatesy et al. 1996). While the origins of Cetacea are becom-ing clearer, the phylogenetic position of Mesonychidae is now as uncertain as ever. Although recent analyses (Geisler and Uhen 2003, 2005) place Mesonychia (Mesonychidae + Hapalodectidae) as the sister-group to a clade that includes Cetartiodactyla and Perissodactyla (but see analyses of The-wissen et al. 2001; Theodor and Foss 2005), this result may be an artifact of the limited number of "condylarth" mam-mals sampled in these studies.

The objectives of the present study are to describe and di-agnose a new species of *Dissacus* from Mongolia and to ascer-tain its evolutionary relationships by conducting a phylogen-etic analysis of Mesonychia. The broader question of the phylogenetic position of Mesonychia within Mammalia is be-yond the scope of the present project, but it is hoped that the phylogenetic information presented in the current study will be incorporated into ongoing efforts to determine the higher-level phylogeny of Eutheria using morphological data (e.g., Asher et al. 2003; Horovitz 2004).

Institutional abbreviations.—AMNH, American Museum of Natural History, New York, USA; IVPP, Institute of Verte-brate Paleontology and Paleoanthropology, Beijing, China; MAE-BU, Mongolian Academy of Sciences and American Museum of Natural History Joint Expedition-Bumban, spe-cimens currently housed at AMNH; USGS, Palaeontology and Stratigraphy Branch, US Geological Survey, Denver, Col-orado, USA; YPM-PU, Princeton University collection at Yale Peabody Museum, New Haven, Connecticut, USA.

Phylogenetic methods

We conducted a cladistic analysis of 19 taxa scored for 89 morphological characters to determine the phylogenetic po-sition of *Dissacus zanabazari* (Appendices 1–3). The major-ity of characters employed came from Geisler (2001), which in turn relied heavily on several previous studies (e.g., Zhou et al. 1995; Geisler and Luo 1998; O'Leary 1998a). Of the 186 characters in Geisler (2001), only those characters that were informative for the 19 taxa sampled in the present study were included. The ingroup includes 14 mesonychians: 12 mesonychids and 2 hapalodectids. All ingroup taxa are mem-bers of Mesonychia, which is monophyletic in several recent studies (e.g., O'Leary 1998a; Geisler and Uhen 2003, 2005; Theodor and Foss 2005). In some previous studies (e.g., Geisler 2001), Cetacea was closely related to a subset of mesonychians, rendering the latter group paraphyletic; how-ever, this conclusion is not supported by molecular studies (e.g., Gatesy et al. 1996; Shimamura et al. 1997; Matthee et al. 2001) or more recent morphological studies (Geisler and Uhen 2003, 2005; Boisserie et al. 2005) that include Cetacea within Artiodactyla.

Six outgroups were used to root the most parsimonious trees: *Andrewsarchus*, *Arctocyon*, *Eoconodon*, and the artio-dactyls *Diacodexis pakistanensis* and *D.* cf. *metsiacus*. Ac-cording to recent cladistic studies, these taxa fall outside Mesonychia (O'Leary and Geisler 1999; Geisler and Uhen 2003, 2005). Cetaceans were not included as outgroups be-cause they no longer appear to be closely related to Meso-nychia (Gingerich et al. 2001). Of the 89 morphological characters, 32 multistate characters are ordered based on similarity between character states (Wilkinson 1992). To find the most parsimonious trees, the matrix was analyzed using the computer program NONA1.9 (Goloboff 1993). Three searches were conducted: (1) heuristic searches using TBR branch-swapping (hold/5; mult*20), (2) trees obtained from the first analysis were used in conjunction with the par-simony ratchet (Nixon 1999) (nixwts*1000), and (3) further branch-swapping on all shortest trees (max*). Bremer sup-port (1988) was determined using the programs TreeRot (Sorenson 1996) and PAUP* (Swofford 2002), with modifi-cations to the TreeRot-generated command file as described by Geisler (2001).

Systematic paleontology

Class Mammalia Linnaeus, 1758
Order Mesonychia Matthew, 1937
Family Mesonychidae Cope, 1875
Genus *Dissacus* Cope, 1881
Dissacus zanabazari sp. nov.
Figs. 1–11, Tables 1–4.

Holotype: MAE-BU-97-13786 (Figs. 1–11), partial skeleton including skull with mandibles; 5 vertebrae: atlas, axis, 2 posterior lumbar, and the first sacral; partial right humerus and ulna; right radius; complete distal left forelimb except for distal phalanges; pelvis, complete right hind limb except for distal ends of metatarsals and distal phalanges; proximal end of left femur. Collected on August 23, 1997 by the joint expedition of the Mongolian Academy of Sciences and the American Museum of Natural History.

Type locality: Tsagaan Khushuu (Tsagan Khushu), Nemegt Basin, Omnogov Aimag (Province), Mongolia.

Derivation of name: In honor of Undur Geghen Zanabazar (1635–1723), a renowned leader of Mongolia who initiated a renaissance in Mongolian religious art, literature, and architecture.

Age and distribution.—The holotype and only known speci-men of *Dissacus zanabazari* was found several meters above the base of the Bumban Member of the Naran-Bulak Forma-tion. Dashzeveg (1988) correlated the mammalian fauna of the Bumban Member with early Eocene faunas of North America and Europe. An early Eocene age for the Bumban fauna is also supported by the faunal cluster analysis of Meng and McKenna (1998).

Diagnosis.—Short face; trilobed lower incisors; no diastemata between lower premolars and molars except between p1 and p2; m3 metaconid subequal to protoconid; lingual face of M3
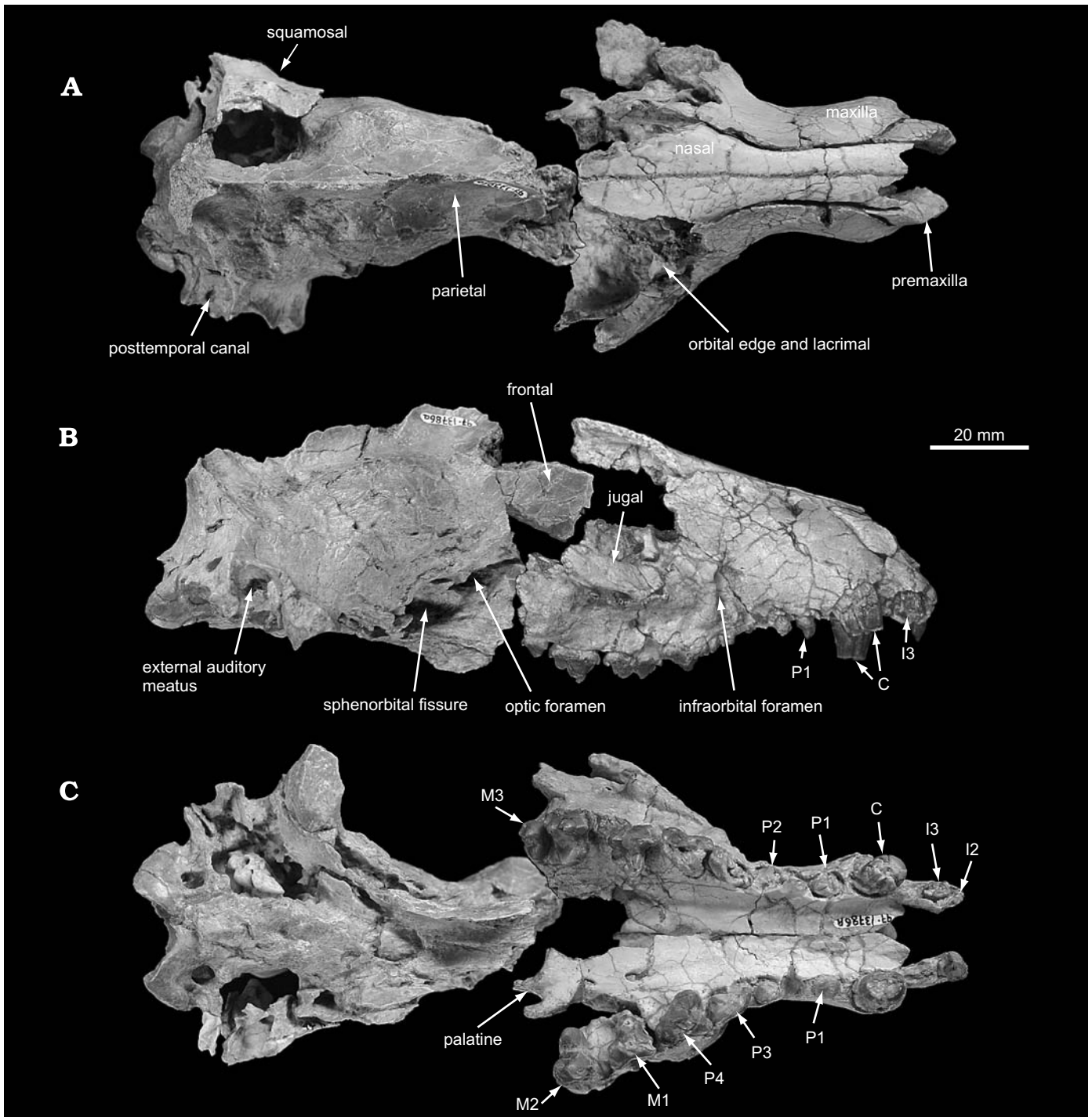
Fig. 1. Skull of *Dissacus zanabazari* sp. nov., holotype, MAE-BU-97-13786, Tsagaan Khushuu, Gobi Desert, Mongolia, early Eocene, in dorsal (**A**), lateral (**B**), and ventral (**C**) views. The antorbital and postorbital portions of the skull are completely separate and were positioned based on more complete mesonychid skulls.

protocone nearly vertical; foramen for superior ramus of stapedial artery entirely within petrosal; anterior halves of 3rd and 4th metacarpals abut each other; medial edge of lesser trochanter of femur not thickened. In addition to the above listed autapomorphies, *Dissacus zanabazari* differs from *D. argenteus* in having a wider talonid basin on m3; differs from *D. europaeus* in having lower hypoconids on p4 and m1–m3,

a transversly wider and mesodistally shorter talonid on m3; differs from *Yantanglestes feiganensis* (originally assigned to *Dissacus*) in having a double-rooted p2, the anterior edge of the orbit over M1 not M2; differs from *D. indigenus* in having a higher hypoconid and cristid obliqua on lower molars, less retroflexed p4 protoconid; differs from *D. serratus* in having higher and less recurved protoconids on p3 and p4, shorter

talonid basin on p3; differs from *D. magushensis* in lacking an entoconid on m1; differs from *D. navajovius* in having better developed talonid basins on p3 and p4, molar protoconids more distal than metaconids, protocone more mesial than paracone on P4; differs from *D. praenuntius* in lacking ento- and ectocingula on m3 and a well-developed metastyle on M3; differs from *D. rotundus* in having a much wider talonid basin on m3; differs from *D. willwoodensis* in having a much wider m3, mandibular ramus that does not deepen posteriorly; differs from *D. argenteus* in having a wider talonid basin on m3; differs from *D. zengi* in being larger and in having a lower hypoconid on m2.

Description

Skull shape.—The skull of *Dissacus zanabazari* has a relatively short face (Fig. 1); as measured along the sagittal plane, the portion of the skull anterior to the orbits forms approximately 38 % of the estimated total condylobasal length (Table 1). It has a pronounced sagittal crest and an elongate and narrow intertemporal region that is less than half the width of the maximum width of the palate. Although not well preserved, it appears that posterior to the orbits, the dorsal edge of the skull was horizontal or sloped posteroventrally.

Premaxilla.—Although the facial portions of both premaxillae are preserved, their palatal portions are not. I2 and I3 are not aligned anteroposteriorly, instead the latter is immediately posterolateral to the former. I3 is significantly larger than I2, and the former is separated from the canine by a distinct diastema (ca. 7.8 mm long, left side). The premaxilla

Table 1. Measurements of the skull and mandible of the holotype of *Dissacus zanabazari* (MAE-BU-97-13786) in mm. Height refers to dorsoventral depth. Abbreviations: Max, maximum; *, estimated; ¥, approximately.

Condylobasal length	160*
Length of face	60.8
Max. width across nasals	18.3
Palate width at P2	29.9
Palate width at M2	51.2
Skull height at M2	47¥
Max. skull width at canines	30.8
Max. skull width at glenoid fossae	65*
Max. skull width at exoccipitals	46.4
Max. width across occipital condyles	31.6
Width of petrosal promontorium	6.8
Max. foramen magnum width	13.9
Max. foramen magnum height	18.4
Right mandible height at p3	16.4
Left mandible height at p3	16.8
Right mandible height at m3	23.2
Left mandible height at m3	20.9

does not form any part of the alveolus for the canine. On the internal surface of the right premaxilla, 1/3 of the way up from ventral margin of this bone, is a longitudinal ridge. This ridge is a continuation of the maxillary crest for the maxilloturbinate. In lateral view, the anterior edge of the premaxilla is inclined posterodorsally and slightly concave. The nasal process of the premaxilla narrows posteriorly to a point and terminates at the level of the posterior edge of the alveolus for the canine (Fig. 1B). Posteriorly, the premaxilla is sutured to and slightly overlapped by the maxilla.

Maxilla and jugal.—Both maxillae are well preserved except that in the right one the region surrounding M3 is missing. In ventral view, the anterior edges of the maxillae together form a "V" shape with the apex pointing posteriorly and centered on the sagittal plane (Fig. 1C). This V-shaped emargination probably received the right and left palatal processes of the premaxillae and the incisive foramina. Anteriorly, the lateral walls of the palate are parallel but then diverge at the level of the P3/P4 diastema. The sides of the palate posterior to P4 are straight, not bowed laterally. The palate is fairly flat. The rostrum is relatively short with teeth that abut one another or are separated by narrow diastemata. P3 contacts P4, M1 overlaps P4, and the remaining teeth are separated by diastemata that are < 5 mm in length. The palatal part of the maxilla is sutured to the palatine posteriorly and medially. The maxilla/palatine suture is L-shaped with a transverse anterior portion and a longitudinal posterior portion that passes just medial to the roots of M2 and M3. Crossing the suture is a longitudinal sulcus for the major palatine artery, vein, and nerve. This sulcus extends to a point medial to the canine. Between the protocones of P4, M1, and M2 are embrasure pits for the lower teeth.

The maxilla articulates with the premaxilla anteriorly; the nasal dorsally; and the jugal, lacrimal, and frontal posteriorly. In lateral view, the maxilla/nasal suture begins at the level of the canine, ascends posteriorly to reach its highest point over P3, and then descends posteriorly to end at a triple junction between the nasal, frontal, and maxilla (Fig. 1B). On the lateral face of the maxilla is a large, dorsoventrally elongate fossa. This fossa leads into the infraorbital canal, which begins dorsal to the posterior half of P3. Dorsal to the infraorbital foramen, the maxilla is gently concave. The dorsoventral thickness of the maxilla ventral to the zygomatic process is quite small. The maxilla does contribute to the orbital mosaic. Not much of the jugal is preserved but its anterior termination is at the level of the small overlap between M1 and P4.

The internal surface of the maxilla is divided into dorsal and ventral halves by the crest for the maxilloturbinate. This crest is oriented anteroposteriorly, turns ventrally at the level of P2, and ends near the floor of nasal cavity at the level of P3. Medial to the infraorbital canal is a dorsoventrally elongate maxillary sinus. The dorsal edge of the sinus is formed by the dorsal ethmoidal crest, which articulates with the lateral plate of the ethmoid bone. A small fragment of the lateral plate is still attached to the left maxilla.
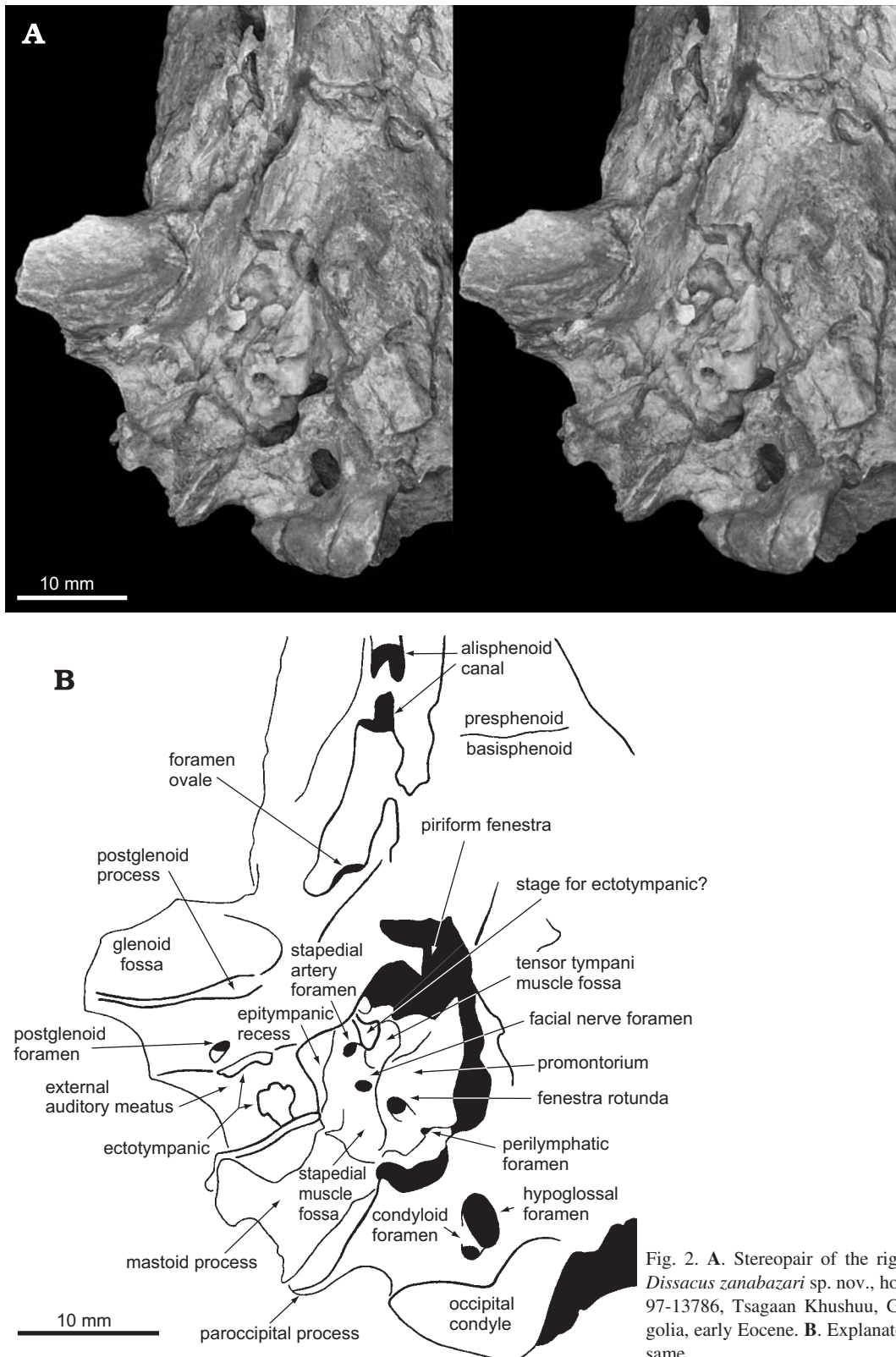
Fig. 2. **A**. Stereopair of the right basicranium of *Dissacus zanabazari* sp. nov., holotype, MAE-BU-97-13786, Tsagaan Khushuu, Gobi Desert, Mongolia, early Eocene. **B**. Explanatory drawing of the same.

Palatine.—Most of the left palatine is preserved while most of the right is not (Fig. 1C). The palatal surface of the palatine is flat, and near its anterior margin is the major palatine foramen. An elliptical minor palatine foramen occurs 6.4 mm posterior to the major palatine foramen. The posterior edge of the palatine bears a prominent post-palatine notch, although an imperfectly preserved post-palatine foramen is possible. The hard palate begins at the level of the M3/M2 contact.

In the orbital mosaic, the palatine contacts the maxilla ventrally along a horizontal suture and the lacrimal anteriorly along a vertical suture. A short distance posterior to the lacrimal suture is a large recess for the sphenopalatine and caudal palatine foramina, which are separated by a small bridge. The former foramen is much larger than the latter. The internal surface of the palatine lacks a sphenoethmoid lamina.

A portion of the palatine is preserved with the posterior half of the skull. It articulates posteriorly with the sphenoid bone, although the exact position of the suture is unclear. In ventral view, the roof of the nasopharyngeal cavity has a transverse suture that separates the palatine anteriorly from the pterygoid posteriorly.

Nasal.—With the skull in dorsal view, the nasals extend from a point over the anterior edge of the canine to terminate between the orbits (Fig. 1A). The anterior margin of left nasal is emarginated, while the right nasal is broken. The rostral portion of the nasals has a flat dorsal surface. The nasal width is narrowest at the level of P2 and widest over P4. Laterally, the nasal articulates with, from anterior to posterior, the premaxilla, maxilla, and frontal. Internally, the medial edge of the nasal bears the septal process, the lateral edge joins the maxilla to form the ethmoidal crest for the dorsal nasal concha, and between these crests is a trough for the dorsal nasal meatus. At the level of P3, the ethmoidal crest turns medially and converges with the septal process to form a median protuberance. Entrenched above this protuberance is the anterior margin of the ethmoidal fossa, which probably received the lateral mass of the ethmoid.

Lacrimal.—The orbital portion of the lacrimal is sutured to the palatine posteriorly and the maxilla ventrally, while the facial portion is broadly overlapped by and sutured to the jugal. Anterior to the orbit, the lacrimal is depressed. We think that the lacrimal was originally flush with the maxilla and was subsequently damaged. If so, the facial exposure of the lacrimal equaled 50% of the anteroposterior diameter of the orbit. The frontal process of the lacrimal is well developed; therefore, the lacrimal forms most of the anterior edge of the orbit. The anteriormost point of the orbit is at the level of the anterior edge of M1. This position is unlike most other mesonychids, which have the anterior edge of the orbit over M2. Along the orbit's edge is a lacrimal tubercle. Behind the orbital edge and ventral to the lacrimal tubercle is a tripartite lacrimal fossa. The middle part is largest and includes the lacrimal foramen. The internal surface of the lacrimal receives a lateral extension of the maxillary sinus. A ridge on the lacrimal separates the maxillary sinus from the frontal sinus.

Sphenoid.—The orbital part of the sphenoid region is perforated by the optic foramen, sphenoidal fissure, and foramen rotundum (Fig. 1B). Approximately 12 mm anterior to the optic foramen, a break provides a cross-section of the sphenoid. Inside are paired sphenoidal fossae with a median septum. The optic foramen is 3 mm in diameter and faces primarily anteriorly. Posterodorsal to it is a ridge that continues posteroventrally to become the edge of the sphenorbital fissure and foramen rotundum. The sphenorbital fissure and foramen rotundum are in a common recess, and they are divided by a thin septum, which is dorsolaterally inclined in anterior view. Anterior to the sphenorbital fissure, the ventral side of the sphenoid contacts the pterygoid via a horizontal suture. The alisphenoid canal is only 5 mm in length, and it opens anteriorly into the lateral wall of the canal for the maxillary branch of the trigeminal nerve. Its posterior opening is in a large common recess with the foramen ovale.

The presphenoid was separated post-mortem from the basisphenoid. It is obscured in ventral view by the pterygoids, which contact each other medially along the sagittal plane. The posterolateral edge of the basisphenoid borders the piriform fenestra (Fig. 2). On that edge are two pits. The medial one may be a foramen for the internal carotid foramen; however, the pits on each side of the sphenoid appear different, which suggests they are artifacts of imperfect preservation. Posteriorly, the basisphenoid is separated from the basioccipital by a straight transverse suture, which is in line with the anterior edge of the promontorium. A pair of ventrolateral tuberosities, one on each side, straddles the basisphenoid/basioccipital suture. They probably mark the attachment of the rectus capitus lateralis muscle.

Squamosal and ectotympanic.—The squamosal is sutured to the parietal and the sphenoid anteriorly, the mastoid process of the petrosal posteriorly, and the tegmen tympani of the petrosal medially. What is tentatively identified as a squamosal/sphenoid suture is angled anteroventrally and leads into a region obscured by matrix and broken bone that is situated 7 mm posterior to the sphenorbital fissure. The glenoid fossa is a deep, transversely elongate fossa that faces ventrally and slightly anteriorly (Figs. 1, 2). It is bounded by prominent preglenoid and postglenoid processes. The glenoid fossa is situated slightly ventral to the level of the basisphenoid and basioccipital. Dorsomedial to the postglenoid process and within the anterolateral corner of the cavum tympani is a spherical tympanic sinus. As in *Dissacus navajovius*, there is a minute postglenoid foramen enclosed by the squamosal (Van Valen 1966). The inferior ramus of the stapedial artery, if present, left no osseous trace.

In lateral view, the dorsal edge of the external auditory meatus is nearly flat (Fig. 1B). The meatus was ventrally enclosed by the ectotympanic bulla, not the squamosal, as indicated by two fragments of the ectotympanic meatal tube on the right side of the skull (Fig. 2). With the skull in ventral view, it is clear that the external auditory meatus is significantly shorter, relative to basicranial width, than in later mesonychids (i.e., 33% of width as compared to *Mesonyx*, 46%). The distal and proximal ends of the meatus have nearly the same anteroposterior diameter. The posterior edge of the external auditory meatus is formed by the post-meatal process of the squamosal, which is sutured posteriorly to the mastoid process of the petrosal.

Petrosal.—In ventral view, the promontorium of the petrosal resembles an isosceles triangle with the long axis pointing anteromedially (Fig. 2). The petrosal does not contact the basioccipital medially, resulting in a continuous basicapsular fissure that varies in width. The fenestra cochleae is large, 2.2 mm in diameter, and nearly circular, except for a flattened dorsolateral edge. It faces posterolaterally and slightly ventrally; thus it is visible in ventral view. Extending posterolaterally from the dorsal edge of the fenestra cochleae is a 2–3 mm shelf of bone. A notch on the posterior edge of the petrosal separates this shelf of bone from the posteromedial corner of the promontorium. A small depression on the anteromedial edge of the fenestra vestibuli may mark the path of the stapedial artery. Lateral to the anterior half of the promontorium is the fossa for the tensor tympani muscle, which forms an anteromedially elongate recess. Immediately posterolateral to the fossa for the tensor tympani muscle is the tympanic opening of the facial nerve canal. Lateral to the fenestra cochleae is a broad fossa for the stapedius muscle. The former is separated from the latter by a sharp ridge whose edge is concave in ventral view. Lateral to the fossa for the stapedius muscle, the proximal end of the mastoid process bulges ventromedially. The medial side of the bulge bears a shallow groove for the hyomandibular branch of the facial nerve.

The foramen for the superior ramus of the stapedial artery is completely enclosed by the tegmen tympani of the petrosal, unlike *Mesonyx*, in which the petrosal only forms the medial side of the foramen (Geisler and Luo 1998). In the *Dissacus zanabazari*, the stapedial foramen is 3 mm anterior to and 2 mm ventral to the tympanic opening of the facial nerve. Anteromedial to the stapedial foramen is a wing-like process that probably formed a stage for the anterior crus of the tympanic ring. The epitympanic region of the petrosal is broad; its width is nearly equal to the promontorial width.

The mastoid process of the petrosal is exposed in ventral view. Its length is 80% the promontorial length and the process forms a 160° angle with the sagittal plane. The ventral surface of the mastoid process on either side is not well preserved, suggesting that it was poorly ossified. With the skull in posterior view, the mastoid process is exposed as a narrow strip between the squamosal, exoccipital, and supraoccipital. A large foramen for the arteria diploetica magna (posttemporal canal) is completely enclosed by the posterior face of the mastoid process (Fig. 1A).

On the endocranial side of the petrosal is a large perilymphatic fossa (ca. 3 mm across). It faces posteriorly and slightly medially, and it includes the perilymphatic foramen. Much of the petrosal's endocranial surface is covered by a deep and elongate suprameatal fossa. A 4 mm deep and 3.5 mm wide subarcuate fossa is situated in the posterodorsal end of the suprameatal fossa. Encircling the subarcuate fossa is a trace of the anterior semicircular canal. Posterodorsal to the anterior semicircular canal is a slit-like endolymphatic foramen. Along the endocranial petrosal/squamosal suture are two foramina, a posterior one for the temporal canal and an anterior one for the superior ramus of the stapedial artery.

Table 2. Dental measurements of the holotype of *Dissacus zanabazari* (MAE-BU-97-13786) in mm. Abbreviations: H, maximum height of crown; LL, labiolingual diameter, on lower molars measured across talonids; MD, mesodistal diameter; ¥, approximately; †, as preserved.

Dentition	Left			Right		
	MD	LL	H	MD	LL	H
I2				1.7	2.95	
I3	4.6	5.0	8†			
C	8.7	6.5		8.9	7.25	
P1	4.1	3.7	4.4			
P2	9.0	3.9				
P3	9.7	5.6		9.2		
P4	9.8	9.4	7.3	10.4		
M1				12.1	10.0	
M2	9.8	10.6	6.1	10.4	10.8	7.2
M3				5.8	7.7	4.9
i1	1.7	2.1	2.8	1.5	2.1	3¥
i2	2.2	2.7	3.6	2.1	2.6	2.9
i3	2.4	2.6	3.7	2.3	2.4	3.4
c	8.3	6.7		8.7	6.6	19.4
p1	4.2	3.5	4.7	4.2	3.8	5.0
p2	8.4	5.1		8.4	5.7	
p3	10.8	4.8	7.8	11.3	5.0	8.7
p4	11¥	5.1	8.3	12.4	5.6	9.2
m1	12¥	5.4	9.2	10.7	4.6	
m2	11.5	5.3	9.5	11.4	5.3	
m3	8¥		7.1	8.2	4.5	6.5

Occipital.—The sutures between the basioccipital, exoccipital, and supraoccipital are fused. Where it is unclear which bone is observed, "occipital" is used. Posterior to the petrosal, the anterior edge of the occipital bears an arc-shaped emargination for the jugular foramen. Posteromedial to it is a very large (ca. 4.2 mm wide) common opening for the hypoglossal and condyloid foramina (Fig. 2). The condyloid canal, which presumably transmitted the condyloid vein, is very short and opens inside the foramen magnum near the dorsal end of the occipital condyle. Ventrally, the occipital condyles are well separated. In ventral view, the anterior edge of the condyle posterior to the hypoglossal foramen is emarginated.

In posterior view, the most salient feature of the occipital is a very large foramen magnum. Its dorsoventral diameter is 14.0 mm, or 69% the basioccipital length. On the right side, the dorsal edge of the foramen magnum is interrupted by a thin triangular flange. A flange was probably present on the left side but may have been broken off. The condyles do not have transverse ridges, as in some artiodactyls (Geisler 2001). The portion of the exoccipital lateral to the condyle is small, only 7 mm long, and featureless. The preserved portion of the supraoccipital is broadly convex. It could not be determined if the mastoid foramen is present.
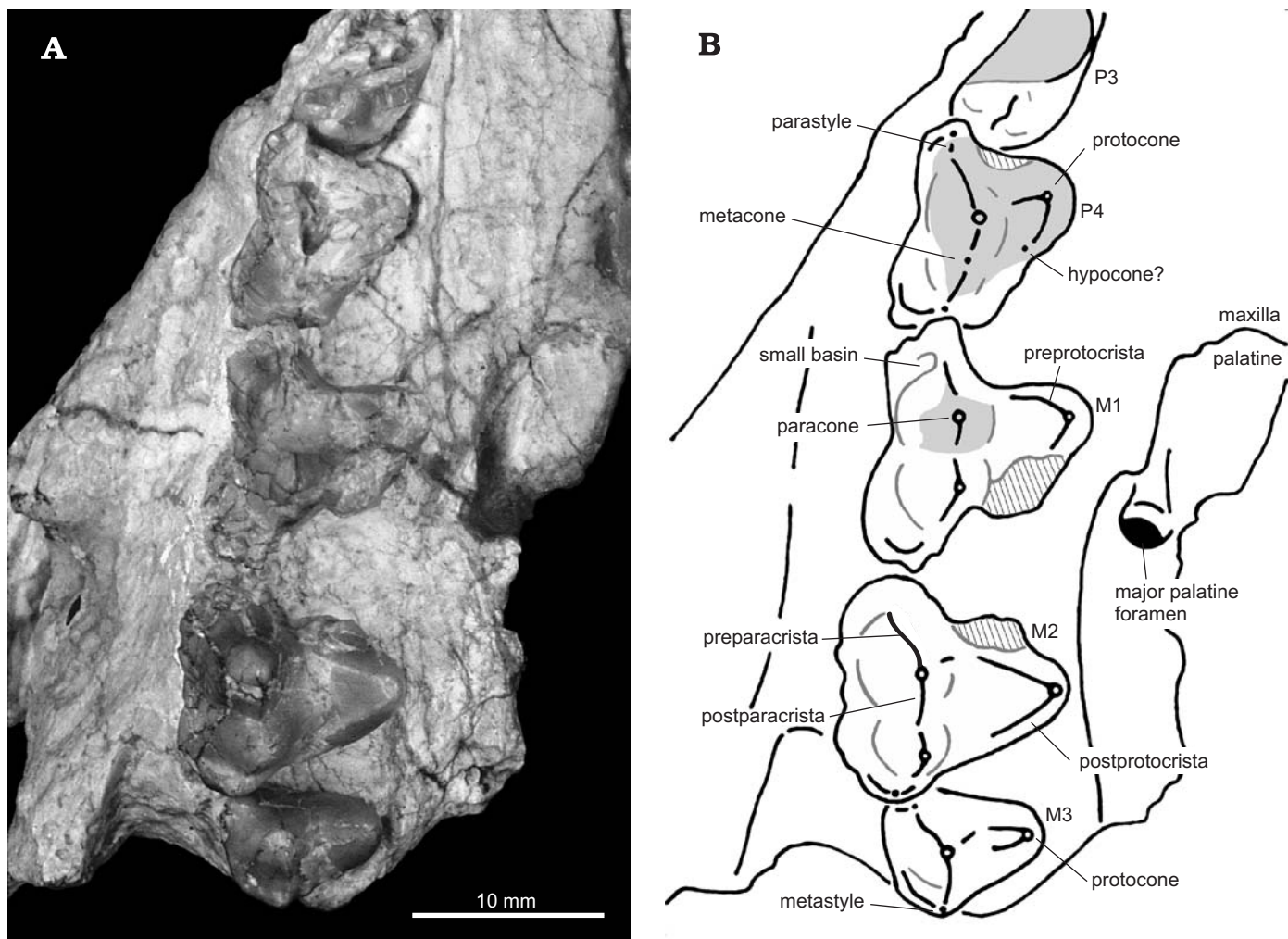
Fig. 3. **A**. Right P4 to M3 of *Dissacus zanabazari* sp. nov., holotype, MAE-BU-97-13786, Tsagaan Khushuu, Gobi Desert, Mongolia, early Eocene. **B**. Explanantory drawing of the same. Hatched areas in B indicate crushed and distorted enamel, and shading denotes missing enamel, with features reconstructed from left dentition.

Upper dentition.—Both I1's are not represented in the holotype, either because they were not preserved or did not occur in this taxon. I2 is only represented by a root missing the crown. I3 is caniniform, single-rooted, and much larger than I2 (Table 2). The canine is the largest tooth of the upper jaw (ca. 8.5 mm anteroposterior diameter). It has an unserrated posterior carina. P1 is a small tooth with one posteriorly hooked cusp (Fig. 1B). The cusp bears anterior and posterior carinae with the former oriented anterolingually. P2 and P3 are badly damaged on both sides. P2 has two roots and bears a low posterior cusp. P3 has two roots, a small parastyle on its anterior corner, and a large protoconid. The preparacrista is absent adjacent to the parastyle and may be absent entirely. The posterior half of the tooth has a central crest.

P4 has a paracone, metacone, protocone, small parastyle, and three roots. The parastyle, preparacrista, paracone, premetacrista, and metacone are aligned anteroposteriorly. The preparacrista joins the paracone and parastyle, while a posterolingually angled postmetacrista joins the metacone and metastyle. Continuing labially from the metastyle is an

ectocingulum that skirts the posterolabial corner of the tooth. A stylar shelf is present but restricted to those portions of the tooth labial and posterior to the metacone (Fig. 3). The metacone is clearly lower than the paracone; however, the precise height difference could not be determined. In labial view, the metacone is indistinct and together with the paracone forms an equilateral triangle.

The protocone of P4 is slightly anterior to the level of the paracone, and the apex of the former is slightly lower than that of the latter. A vertical sulcus on the anterior side of P4 separates the protocone and paracone. The trigon basin faces posteroventrally and is bounded by pre- and postprotocristae that extend away from the protocone's apex. The preprotocrista is at a right angle to the aligned crests between the parastyle and metacone. The postprotocrista is much lower than the preprotocrista and bears a small bulbous cusp that may be a small cingular hypocone. P4 has stylar shelf posterolabial to the metacone.

Both M1's are damaged, so a complete description is not possible. M1 is three-rooted and is dominated by the para-

cone and metacone. The paracone is taller than the metacone, although the exact height difference is unclear. The prepara-crista, premetacrista, and postmetacrista are aligned antero-posteriorly. Just labial to the preparacrista and posterior to the parastyle is a small basin. A poorly defined postmeta-crista extends posteriorly from the metacone and joins a cingulum on the posterolabial corner of the tooth, which may be homologous with the metastyle. The stylar shelf is present on the anterolabial and posterolabial corners of the tooth but is absent from the intervening stretch. The trigon basin is transversely expanded and anteroposteriorly narrow. There is no metastyle or hypocone, but the presence or absence of the parastyle could not be determined. The protocone is di-rectly lingual to the paracone. Extending labially from the protocone is a preprotocrista and posterolabially a post-protocrista.

M2 is approximately the same size as M1. From what can be observed, M1 and M2 are similar. The following descrip-tion focuses on those features that are different from M1 or could only be observed on the better-preserved M2. The paracone is the dominant labial cusp and is approximately twice the height of the metacone. Extending away from the apex of the paracone are a preparacrista and a postparacrista, the latter being better developed than the former. It is unclear if the ectocingulum on the anterolabial corner of the tooth also includes a parastyle. The metastyle is situated on a small ectocingulum that wraps around the posterolabial corner of the tooth. The posterolabial portion of the stylar shelf is not as well developed as the anterolabial portion. The protocone is nearly as tall as the paracone and is situated lingual to the gap between the paracone and metacone. Connecting the paracone and protocone is a crest that is notched down to the level of the trigon basin. The paraconule, metaconule, and hypocone are absent.

M3 is much smaller than both M1 and M2. Relative to its width, the mesodistal length of M3 is small (Table 2). The short length is associated with a simplified compliment of la-bial cusps; M3 lacks a metacone and the parastyle and meta-style are very small. The paracone is the dominant labial cusp of the tooth. It connects to the parastyle via a preparacrista and to the metastyle via a postparacrista. Immediately lingual to the parastyle is a small cusp of uncertain homology. An ectocingulum occurs on the distal half of M3 and is joined by a short crest to the metastyle. The other sides do not have cingula. The trigon basin is elongate transversely and com-pressed anteroposteriorly. Between the paracone and proto-cone is a deeply notched crest that forms the anterior side of the trigon basin. Like the other molars, the paraconule and metaconule are absent. A weakly developed postprotocrista is present. The protocone is fairly bulbous although the base is not expanded lingual to the apex. The protocone is slightly lower than the paracone and the hypocone is absent. Like M1 and M2, M3 has three roots.

Lower dentition and mandible.—The mandibular symp-hysis extends posteriorly to the level of p3 (Fig. 4C). The depth of the mandible below m3 is only slightly greater than its depth below p3. The smallest teeth in the lower dentition are i1, i2, and i3 (in order of increasing size). All three are sim-ilar in morphology with minor variations. In anterior view, each has a narrow base but wider apex. Their crowns have three cusps that have been worn to the same height; a large central cusp and two smaller cusps on either side (Fig. 4A). The crown of i3 is so small that the cusps are indistinct. Labial to lingual cross-sections of the teeth are chisel-shaped.

The canine is the largest of the lower teeth. A poorly de-veloped carina begins on the posterolabial side at the crown base, then gradually traverses across the posterior face of the canine, and ends on the posterolingual side near the apex. A second carina occurs on the anterolingual side of the tooth. Posterior and parallel to the anterolingual carina is a deep but narrow sulcus, which may be a preservational artifact.

The first premolar is a small tooth with a single retro-flexed cusp (Fig. 4B, C). The cusp has an anterior carina on the apical half of the crown and a posterior carina along its entire length. A small pit is located near the base of the crown immediately lingual to the posterior carina. A large proto-conid occurs on p2, although only the base of the cusp is pre-served. The protoconid has well-developed anterior and pos-terior carinae. Posterior to the protoconid is a much lower hypoconid with anterior and posterior crests. In occlusal view, the anterior half of the tooth is much narrower than the posterior half.

The third premolar is dominated by a large retroflexed protoconid that has anterior and posterior carinae. At the base of the anterior carina is a small nub (paraconid?). The poste-rior carina terminates into a carnassial notch. The hypoconid is compressed transversely and bears a crest running along its entire length. Lingual to the carnassial notch and the hypo-conid is a small talonid basin that is not enclosed posteriorly.

The fourth premolar has a protoconid, paraconid, and hypoconid but no metaconid, entoconid, or cingula (Fig. 4B, D). A recurved protoconid is the dominant cusp. A well-de-fined, mesodistal paracristid connects the protoconid to a small but distinct paraconid. Extending posteriorly from the protoconid is a crest, here referred to as the postprotocristid, which terminates at the carnassial notch. The cristid obliqua stretches from the carnassial notch to the hypoconid. Lingual to the cristid obliqua is a large and well-developed talonid basin, which is enclosed posteriorly by a transverse crest.

The protoconid of m1 is closely appressed to the meta-conid, resulting in the appearance of a single large cusp with two apices. The protoconid is immediately posterolabial to the metaconid, and the apices of both are separated by well-defined, dorsoventral grooves. In occlusal view, these grooves are equidistant from the metaconid and protoconid, indicating that the cusps are subequal. The protoconid and metaconid are approximately the same height. The anterior groove opens anterolingually to form a small trigonid basin. Anterior to the protoconid is a paracristid leading to a low paraconid. Extend-ing posteriorly from the protoconid to the carnassial notch is a postprotocristid. The morphology of the posterior half of the
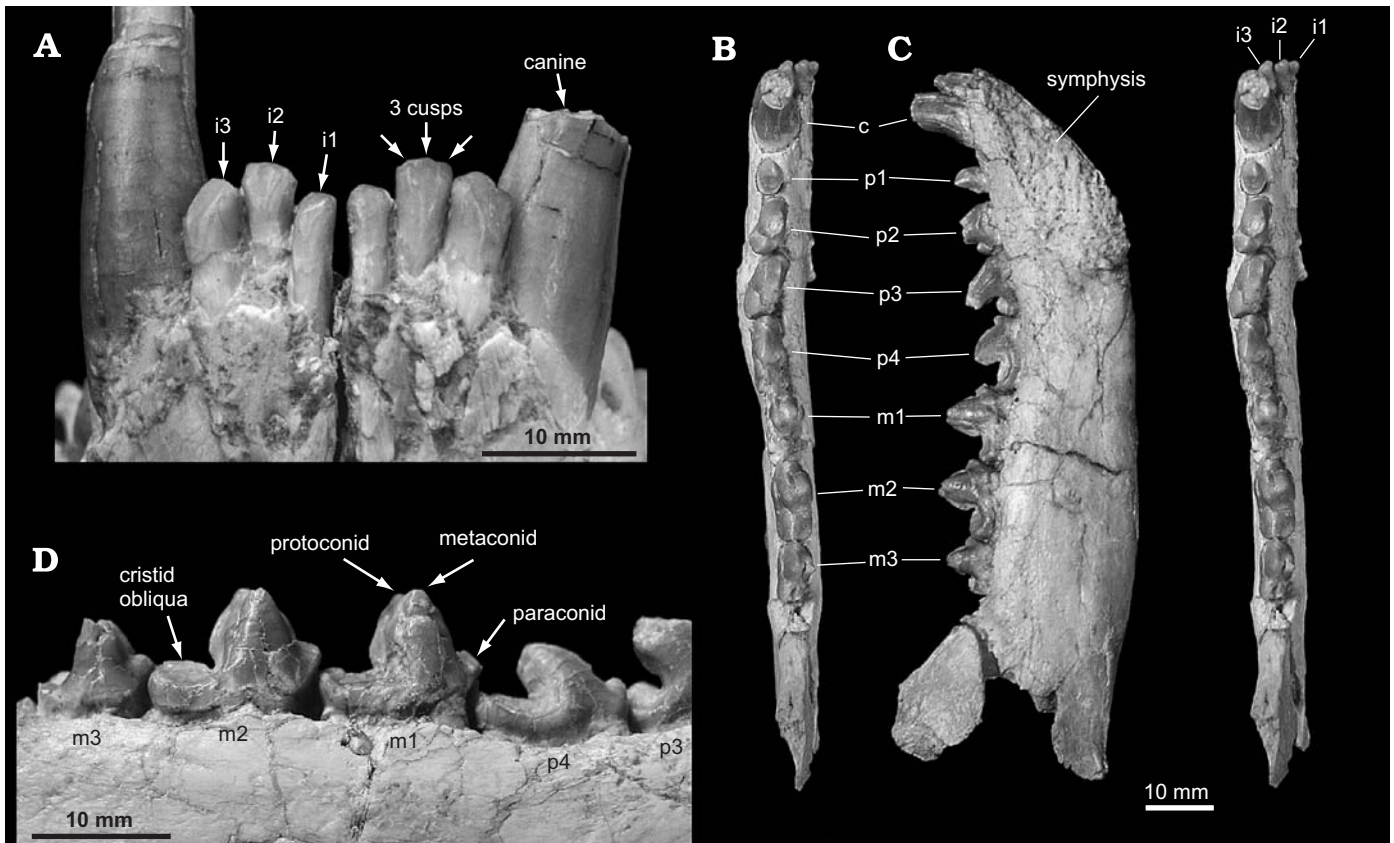
Fig. 4. Mandible and lower dentition of *Dissacus zanabazari* sp. nov., holotype, MAE-BU-97-13786, Tsagaan Khushuu, Gobi Desert, Mongolia, early Eocene. **A**. Anterior view of the lower canines and incisors. Note the weakly trilobed morphology, most evident on i2. **B**. Stereopair of the left mandible in dorsal view. **C.** Medial view of the left mandible. **D**. Lingual view of the left p4 through m3.

tooth is similar to that of p4. The posterior border of the talonid basin is formed by a transverse crest that starts at the hypoconid and wraps around the posterolingual corner of the tooth. In lingual view, the paraconid is slightly higher than the hypoconid, and the protoconid and metaconid are more than twice the height of the hypoconid. The trigonid basin is approximately twice as high as the talonid basin. The first molar lacks cingula, an entoconid, and a hypoconulid.

The left m1 and m2 are approximately the same size; however, on the right side, m2 is slightly larger. The second molar is similar to m1 with differences noted below. On the left m2, the center of the talonid basin has a mesodistal crease with adjacent entocingulid. There is no crease or entocingulid on the right m2. A poorly developed entoconid occurs at the posterolingual corner of the basin.

The third molar is significantly smaller than m2 (Table 2). The protoconid is closely appressed to the metaconid, and the former is labial to the latter. Both cusps are subequal in height and size. Anterior to the protoconid is paracristid with a low paraconid. Ventral to the paraconid the anterior side of the tooth is gently convex, resembling the bow of a ship without a keel. It also has a postprotocristid and cristid obliqua that join at a carnassial notch and a short and poorly developed talonid basin. The third molar lacks an entoconid, hypoconulid, and cingulids. In occlusal view, the base of the tooth is widest across the protoconid and metaconid and narrowest across the carnassial notch. In lingual view, the paraconid is slightly higher than the hypoconid while the protoconid and metaconid are twice the height as the hypoconid. The trigonid basin is elevated as high as the talonid basin.

Vertebrae.—The atlas was recovered; however, it is badly distorted and missing both wings. The dorsal margins of the articular surfaces for the occipital condyles curve inward. Lateral to the dorsal part of the articular surface for the axis is the transverse foramen. The atlas lacks a ventral tubercle on the body and an alar foramen in the wing. It is unclear if the lateral vertebral foramen for the 1st spinal nerve was present.

The anterior 2/3rds of the body of the axis is preserved, as are the pedicles of the neural arch. In anterior view, the articular surface for the atlas resembles a bowtie, centered on the odontoid process. The lateral sides of the articular surface are slightly convex, and in ventral view, each slopes away from the odontoid process at a 120° angle from the sagittal plane. The odontoid process is longer than wide and has a nearly circular cross-section.

Two lumbar vertebrae were found in articulation with the first sacral vertebra. Both lumbars are very similar, and the following description is a composite based on both vertebrae. The centrum is long; its length is nearly 150% its anterior
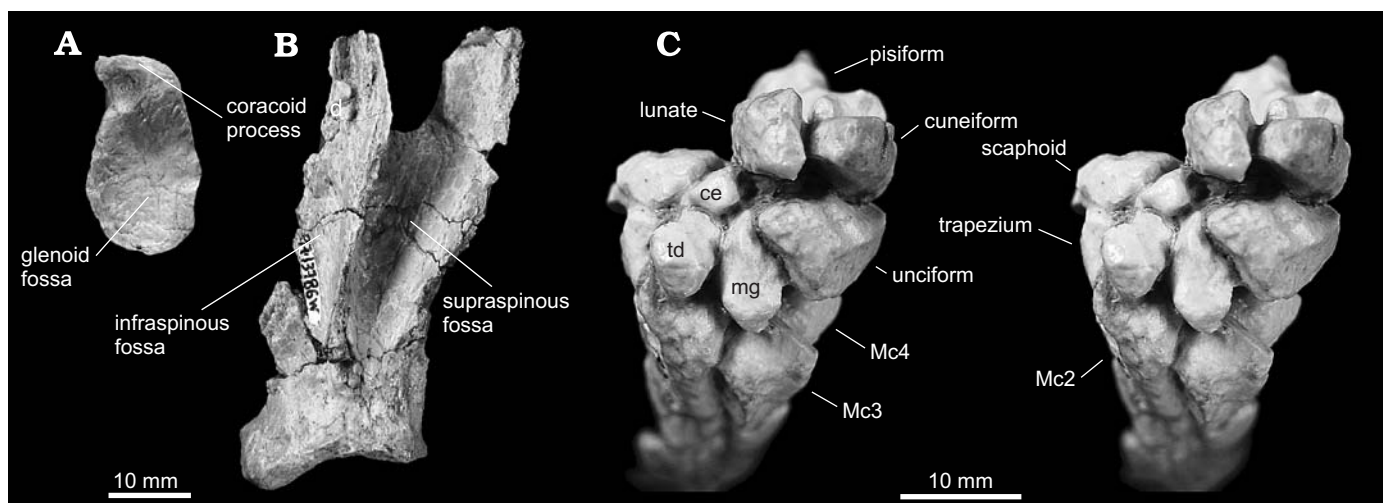
Fig. 5. *Dissacus zanabazari* sp. nov., holotype, MAE-BU-97-13786, Tsagaan Khushuu, Gobi Desert, Mongolia, early Eocene. Left scapula shown in ventral (**A**) and lateral (**B**) views **C**. Stereopair of left manus, in anterior view. Abbreviations: ce, centrale; Mc, metacarpal; mg, magnum; td, trapezoid.

width (Table 3). In anterior view, the centrum is semicircular, with the flat side on the dorsal margin. In ventral view, the transverse processes point anterolaterally, forming 30° angles with the sagittal plane. Although not entirely preserved, there is no indication that the lateral ends of the transverse processes are flared. Rising above the pedicle are robust prezygapophyses with revolute lateral edges. The mamillary processes are poorly developed. What little is preserved of the dorsal edge of the spinous process gradually descends posteriorly. The postzygapophysis bears a highly convex articular surface that faces ventrally and laterally.

Only the first sacral vertebra is preserved. Its centrum is wider than long and bears a weakly defined, median keel on its ventral surface. The anterior half of the neural arch bears a low median sacral crest, which in lateral view is triangular and highest anteriorly. Projecting from the posterior edge of the neural spine is a tab of bone that articulated with the 2nd sacral vertebra. The sacral wing is not very wide, being less than twice the centrum width. The anterior half of the wing bears a large cup-shaped prezygapophysis. As compared to more proximal portions, the distal end of the wing is expanded anteriorly, ventrally, and posteriorly.

Scapula.—Except for the acromion process, only the ventral end of the left scapula was preserved (Fig. 5A, B). The

Table 3. Measurements of the vertebrae of the holotype of *Dissacus zanabazari* (MAE-BU-97-13786) in mm. Centrum width corresponds to the maximum width across the anterior face, or across the lateral bodies for the atlas. The maximum vertebral width includes the transverse processes. Abbreviations: L, length; W, width; †, as preserved.

Vertebra	Centrum W.	Centrum L.	Max. W.
Atlas	29.6		
Axis	10.5		
2nd to last lumbar	14.3	23.1	37.4†
Last Lumbar	14.4	19.5	
1st sacral	16.5	14.2	27.4

anteroposterior width of the preserved portion of the supraspinous fossa is subequal to that of the infraspinous fossa. Although the infraspinous fossa is concave, the medial side of the blade is convex. In ventral view (Fig. 5A), the glenoid fossa is approximately oval-shaped, narrower anteriorly than posteriorly. It is shallow, with a maximum depth of 1.6 mm. The supraglenoid tubercle is well developed, and its extreme anteroventral end bears a broken coracoid process. Between the base of the coracoid process and the edge of the glenoid fossa is a distinct pit, from which the biceps muscle probably originated.

Humerus.—Only the distal 2/3 of the right humerus was preserved (Fig. 6B). The distal articular surface can be divided into a trochlea for the ulna, a capitulum that articulates with the radius, and an articular surface on the lateral epicondyle for the radius. A sharp ridge forms the medial edge of the trochlea, which is also the medialmost edge of the articulating portion of the humerus. While on the anterior side the trochlea is parasagittal, the portion on the posterior face is slightly angled proximolaterally. Proximal to the trochlea and on the anterior and posterior sides of the humerus are deep fossae. They are perforated by an opening that is a supratrochlear foramen or a preservational artifact. The capitulum is smoothly convex and lacks a median sagittal ridge. In distal view, the center of the capitulum leads posteriorly into a sharp crest that forms the lateral trochlear edge. Immediately lateral to the capitulum is a shallow parasagittal groove, and lateral to it is a flat to slightly raised articular surface for the radius. Epicondyles are situated medial and lateral to the distal articular surfaces of the humerus. Although poorly preserved, the maximum width of the medial epicondyle is about 50% the combined width of the distal articulating surfaces. Although the presence or absence of an entepicondylar foramen could not be determined, a supinator crest is present proximal to the lateral epicondyle.
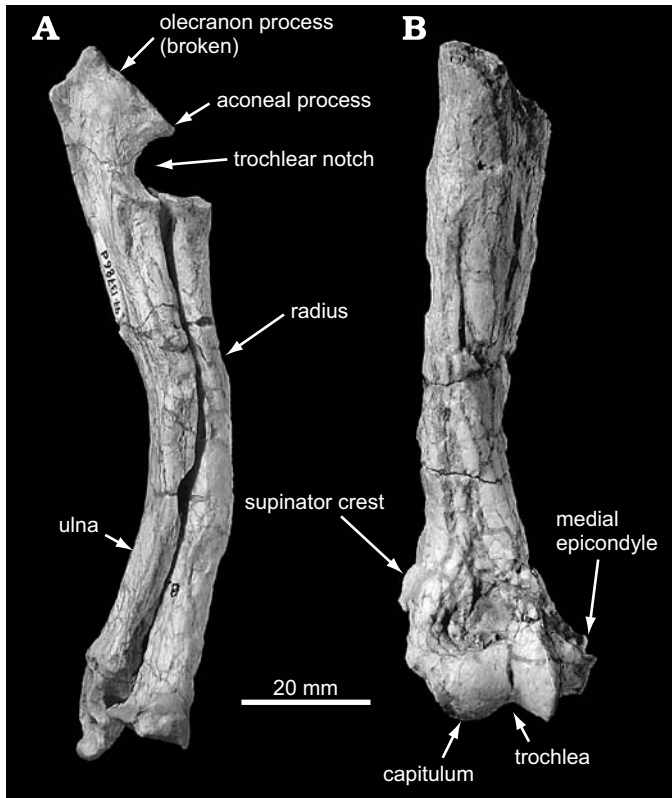
Fig. 6. *Dissacus zanabazari* sp. nov., holotype, MAE-BU-97-13786, Tsagaan Khushuu, Gobi Desert, Mongolia, early Eocene. **A**. Left radius and ulna in medial view. **B**. Right humerus in anterior view.

Ulna.—The entire left ulna, except for the tip of the olecranon process, and the distal half of the right ulna were preserved. Both ulnae were found in articulation with the radii. The left ulna is strongly bowed, in part due to post-mortem deformation (Fig. 6A). The posterior side of ulna is formed by a transversely compressed ridge. Along the lateral side of the ulna is a deep, longitudinal fossa, which likely received the abductor pollicis longus (O'Leary and Rose 1995b). On the distal third of the anterior face of the ulna is a narrow, elongate platform that likely articulated with the radius prior to post-mortem deformation. The suture between the diaphysis and the distal epiphysis is visible, indicating that this individual was not mature.

In lateral view, the trochlear notch for the humerus is C-shaped. This notch is divided into medial and lateral parts by a longitudinal ridge. The larger lateral part is concave, faces distally, and extends onto a flange that projects from the aconeal process. Immediately distal to the articular surface on the lateral side is an oval-shaped pit, which O'Leary and Rose (1995b) labeled the incisure in the semilunar notch. Distal to the incisure is a small medial flange that articulates with the radius. The medial part of the trochlear notch is crescent-shaped, parasagittal, and divided into a proximal, medially-facing portion and a distal, proximally-facing portion. The transition between the proximal and distal parts is gradual. As in *Dissacus navajovius* (AMNH 3359), the proximal

third of the trochlear notch's medial edge is poorly defined. The proximally-facing portion occurs on the coronoid process, which projects anteriorly from the distal end of the trochlear notch. On the medial side of the ulna and posterior to the trochlear notch is a longitudinal fossa, probably for a deep digital flexor as in *Canis* (Evans 1964).

Radius.—Both the right and left radii were recovered; however, only a small fragment of the left distal epiphysis was found. The diaphysis of the radius is bowed anteriorly (Fig. 6A). Its proximal end bears a tripartite articular surface for the humerus: a concave and oval central portion for the capitulum; a flat, proximomedially-facing facet for the medial side of the trochlea; and a flat, proximolaterally-facing facet for the lateral epicondyle. The highest part of the proximal face is on the posterior edge of the radius, at the junction between the middle and lateral parts of the humeral articulation surface.

A broad fossa for the supinator muscle occurs on the lateral 2/3rds of the anterior face of the radius, just distal to the proximal end of the radius. On the posterior face of the radius and along the distal third of the diaphysis is a pair of longitudinal ridges, with an intervening fossa. The interosseous membrane likely attached to the lateral of the two ridges. The distalmost, preserved part of the diaphysis is inflated, with a transverse width more than twice that of the midshaft.

Carpals.—The manus is described based on the inferred digitigrade posture of *Dissacus*; therefore, the palmar aspect of most bones faces posteroventrally. The proximal face of the scaphoid has a facet for the radius that is convex anteroposteriorly; nearly flat transversely; and rectangular in shape, with the long axis oriented anterolaterally to posteromedially. Posterior to the radial facet is a large fossa that occupies most of the proximal surface. Posteromedial to this fossa is a bulbous scaphoid tubercle. Distally, the scaphoid articulates with three bones: from medial to lateral they are trapezium, trapezoid, and centrale (Fig. 5C). In anterior view, the distal margin of the scaphoid is gently convex as in *Ankalagon* (AMNH 777). The lateral side of the scaphoid likely articulated with the lunate.

In medial view, the trapezium has four sides: a proximal side that contacts the scaphoid, an anterior side that contacts the trapezoid and 2nd metacarpal, a distal side that contacts the 2nd metacarpal, and a posterodistal side that contacts the 1st metacarpal (Fig. 7). In anterior view, the trapezoid has a V-shaped distal margin, which fits into a corresponding trough on the 2nd metacarpal. The anterior surface of the trapezoid is highly convex but does not bear a distinct protuberance as in *Pachyaena* (Rose and O'Leary 1995; AMNH 16154) and *Ankalagon* (AMNH 777). Its proximal surface articulated primarily with the scaphoid but also with the centrale. The medial side is flat proximodistally, concave anteroposteriorly, and articulated with the trapezium.

The centrale is the smallest carpal bone. In anterior view, it is roughly diamond-shaped except that the proximomedial
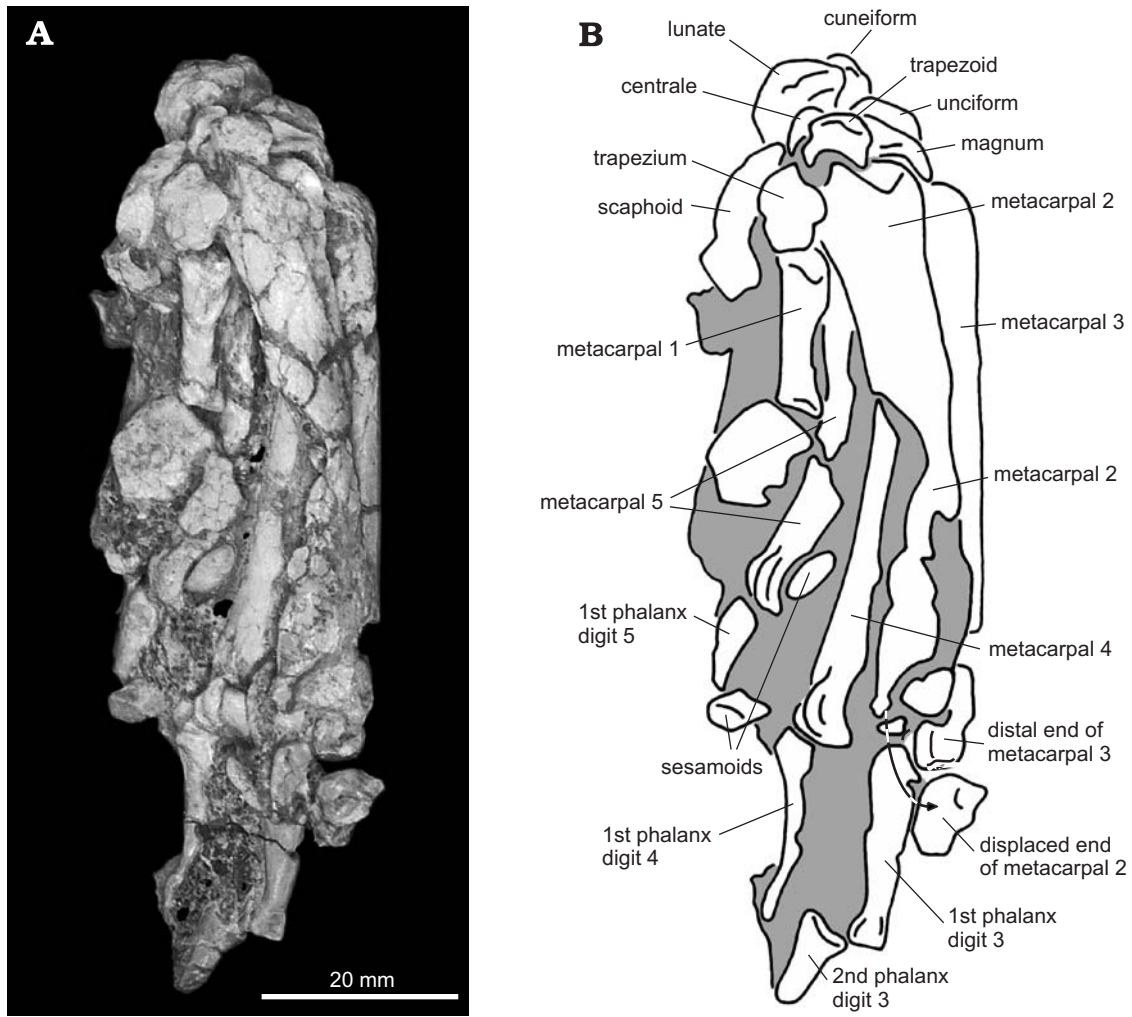
Fig. 7. **A**. Medial view of the left manus of *Dissacus zanabazari* sp. nov., holotype, MAE-BU-97-13786, Tsagaan Khushuu, Gobi Desert, Mongolia, early Eocene. **B**. Explanatory drawing of the same.

side is longer than the distolateral side (Fig. 5C). The overall size of the centrale in *Dissacus zanabazari* is proportionally larger than in *Pachyaena* but similar in proportion to that of *Ankalagon* (AMNH 777). It appears to have partially separated the scaphoid and trapezoid. The proximomedial surface of the centrale articulates with the scaphoid, proximolateral surface with the lunate, distolateral with the magnum, and the distomedial with the trapezoid.

The anterior face of the magnum is triangular and pointed distally. Whereas in *Pachyaena* the anterior face of the magnum is larger than the trapezoid, the opposite is true in *D. zanabazari*. The proximal surface of the magnum is bisected by a median ridge, which divides a medial centrale facet from a lateral lunate facet. Posterior to the facet for the centrale, the magnum articulated with the trapezoid. This differs from *Pachyaena* (AMNH 16154) where the magnum articulates with the trapezoid on its medial, not proximal, surface. The medial side of the magnum articulates with the 2nd metacarpal, the pointed distal side with the 3rd metacarpal, and the lateral side with the unciform.

In anterior view, the lunate is much taller than wide (Table 4). The lunate articulated with the scaphoid and centrale medially, the magnum and unciform distally, the cuneiform laterally, and the radius proximally. Only the contacts with the cuneiform and centrale remain after post-mortem, partial disarticulation. The anterior half of the cuneiform facet is concave, similar to *Ankalagon* (AMNH 777) but not like *Harpagolestes* (AMNH 1945). The facet for the radius is restricted to the anterior third of the proximal surface. On the distal face of the lunate is a sharp ridge that separates a larger flat to convex facet for the magnum from a smaller concave facet for the unciform.

The unciform has the largest anterior face of all carpals. In anterior view, it is shaped like half of a circle with a flat proximal edge and a bowed distal edge. The proximal surface of the unciform articulated with the cuneiform laterally and the lunate medially; however, unlike other mesonychids (e.g., *Harpagolestes*, AMNH 1945) there is no ridge separating the two facets. The facet for the cuneiform is the larger of the two. The medial side articulated with the magnum and

the 3rd metacarpal. Like *Ankalagon* (AMNH 777), the distal surface has a single large concave surface that articulated with the proximal end of the 4th and 5th metacarpals.

The cuneiform is much wider than tall. Its proximal face has a transversely flat and anteroposteriorly concave facet for the styloid process of the ulna. The anterior edge of the facet is straight, not curved as in other mesonychids (e.g., *Pachyaena*, AMNH 1615; *Harpagolestes*, AMNH 1945). Immediately posterior to the ulnar facet is a pisiform facet that faces, in part, posteriorly. Lateral to the pisiform facet is the posterolateral process (sensu O'Leary and Rose 1995b). The distal side of the cuneiform articulates with the unciform and the medial side with the lunate.

The proximal end of the pisiform is saddle-shaped, being concave transversely and convex proximodistally. Its proximal part articulated with the styloid process of the ulna while the distal part articulates with the cuneiform. The ulnar and cuneiform facets are continuous except for a low ridge, which is restricted to the extreme lateral side of the pisiform. These facets in other mesonychids are completely separate (Rose and O'Leary 1995). The posterior end of the pisiform is expanded and has a smooth, concave surface of unknown function.

Metacarpals.—The manus is paraxonic; 3rd and 4th metacarpals are subequal in length. The 1st metacarpal is substantially smaller than the other metacarpals and points posterodistally away from the rest of the manus (Fig. 7, Table 4). Its proximal end articulates with the trapezium and originally with the 2nd metacarpal. The distal end of the 1st metacarpal is not keeled, flat transversely, and convex anteroposteriorly. Although poorly preserved, the 2nd metacarpal is clearly much larger than the first. The proximal side of the 2nd metacarpal articulates with, from medial to lateral, the trapezium, trapezoid, magnum, and 3rd metacarpal. The proximal end of the 2nd metatarsal is more proximal than the other metacarpals.

Even though the distal ends of the 3rd and 4th metacarpals are aligned, the 3rd is the longer of the two (Table 4). It appears that the 3rd and 4th metacarpals articulated with each other for most if not all of their length. The 3rd metacarpal articulates proximally with the magnum and unciform. Its shaft is roughly rectangular in cross-section. The 3rd's distal end is slightly wider than the shaft, cylindrical in shape, and bears a median keel. The medial and lateral sides of its distal end bear prominent pits. Although no sesamoids are articulated, at least four occur in the surrounding matrix. The 4th metacarpal is quite similar in overall morphology to the 3rd. Its proximal end articulated with the unciform and its anterior face is gently convex, not flattened. The 5th metacarpal articulates proximally with the unciform, has an anterolateral instead of an anterior side, and has a stout diaphysis.

Pelvis.—Much of the pelvis was preserved except for its anterior edges and the parts surrounding the pubic symphysis. The wings of the ilia are vertical, with little of their lateral surfaces visible in dorsal view. In dorsal view, the ilia diverge at an angle of 50°. Along the medial side of the ilium is

Table 4. Measurements of the limb bones of the holotype of *Dissacus zanabazari* (MAE-BU-97-13786) in mm. For the astragalus, transverse width of the proximal end includes the lateral process, and for the calcaneus, the end of the tuber is considered distal while the articulating portion is considered proximal. The proximal and distal dimensions of small carpals and tarsals are virtually the same. Abbreviations: AP, anteroposterior diameter; Dist., distal end; l, left; L, length; mc, metacarpal; Mid., middle of shaft or bone; mt, metatarsal; Prox., proximal end; r, right; T, transverse diameter; †, as preserved; ¥, approximately.

Bone	L	Prox. AP	Prox. T	Mid. AP	Mid. T	Dist. AP	Dist. T
r-humerus						19.5†	31.3†
l-ulna	116.2†			11.0	10.8		
l-radius	89.5†	9.6	15.1				
r-radius		8.7	13.6				
l-cuneiform	5.2		11.9				
l-unciform	7.4		11.7				
l-lunate	7.2	10¥	5.6				
l-scaphoid	4.7	12¥	8.9				
l-mc 1	15.1				2.9	3.92	4.1
l-mc 2			7.9				
l-mc 3	46¥		7.7	5¥	5.0		
l-mc 4	44.9		6.6		5.5¥		
l-mc 5	33.9				6¥		
r-femur	139.9	22.7	28.5	16.0	11.5		23.3
r-tibia	132.8	27.6	24.0†	12.9	11¥		
r-fibula						11.37	7.3
r-astragalus	20.3		14.8			9.26	11.3
r-calcaneus	36.5		12.8				9.6
r-navicular	15.7†	10.7	12.7				
r-ectocuneiform	6¥	5.8	5.0				
r-mt 1	6.0	2.8					
r-mt 2			8.3				
r-mt 3		11.3	6.3				
r-mt 4		9.4	6¥				
r-mt 5			6.7				

a broad region that is sutured to the sacrum. In lateral view, the dorsal edge of the ilium is sigmoidal with a convex portion between the anterior and posterior dorsal iliac spines, followed by a concave part at the greater ischiatic notch, and finally a convex region that ascends towards the ischiatic spine (Fig. 8A).

In lateral view, the acetabulum is circular with a high rim. Its lunate articular surface opens posteroventrally, and the ends of the articular surface are separated by a 6.5 mm gap. Extending anteriorly from the edge of the acetabulum is an elevated, broad rugosity. In its center is an oval pit that subdivides the rugose region into dorsal and ventral ridges. The smaller dorsal ridge is probably for the articularis coxae muscle and the larger ventral one is probably for the rectus femoris. A broad, longitudinal ridge runs from the posterior
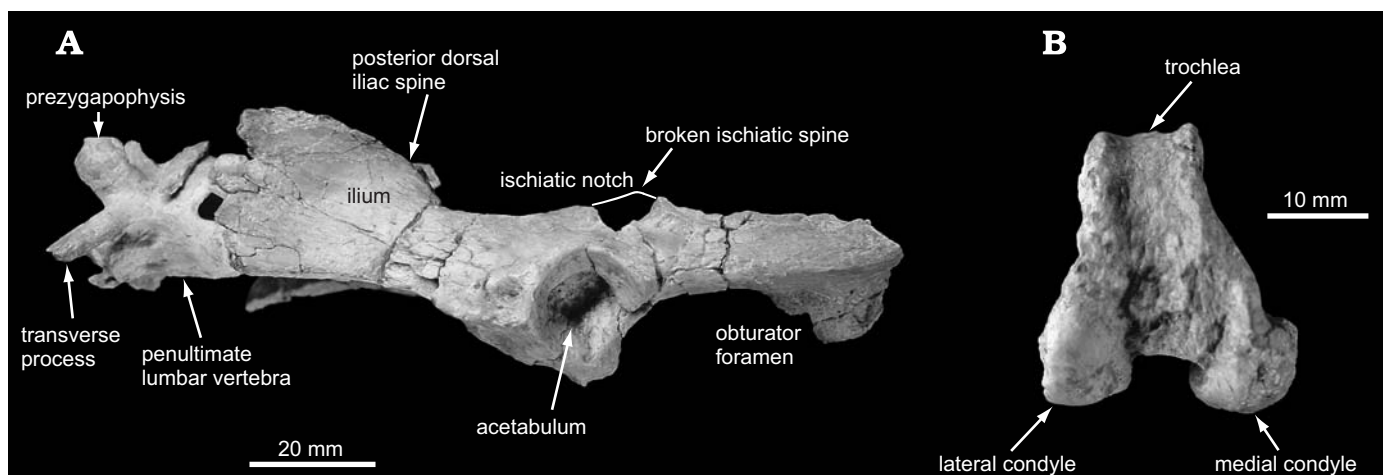
Fig. 8. *Dissacus zanabazari* sp. nov., holotype, MAE-BU-97-13786, Tsagaan Khushuu, Gobi Desert, Mongolia, early Eocene. **A**. Lateral view of pelvis with lumbar and sacral vertebrae. **B**. Right femur in distal view.

edge of the acetabulum to the posteriormost part of the preserved ischium. Above the ridge the ischium faces dorsolaterally and below it the ischium faces ventrolaterally. Along the dorsal edge of the ischium is the ischiatic spine, which is directed dorsolaterally.

Femur.—The entire right femur and the proximal 2/3rds of the left femur were recovered. The right femur is more bowed anteriorly and, as with other forelimb elements, this is attributed to postmortem deformation. A shallow ligamental fovea occurs on the femoral head, and it is entirely encircled by the articular surface. Opposing the head is the greater trochanter, which extends to the same proximal height as the head of the femur (Fig. 9A). Distal to the proximal end of the humerus are the lesser and third trochanters. Unlike other mesonychids (e.g., *Ankalagon saurognathus*, AMNH 776), the lateral edge of the lesser trochanter is thin, not thickened. The third trochanter is centered at the boundary between the proximal and middle thirds of the femur. The distal end of right femur is highly corroded, particularly on the medial and lateral sides. Even with the poor preservation, the distal end clearly has a high and narrow trochlea (Fig. 8B). Posterior to the trochlear edges are ovoid femoral condyles, which face posterodistally and are separated by a 5 to 6 mm wide intercondyloid fossa. Whereas the lateral condyle is nearly even in width and parasagittal in orientation, the medial condyle is wider proximally and is oriented proximolaterally.

Tibia.—A complete right tibia was collected (Fig. 9B), but the left tibia was not found. On the proximal face of the tibia, the medial articular surface is inferior to the lateral one. The lateral articular surface for the femur is nearly circular in shape, concave transversely, flat anteroposteriorly, and bounded medially by one of two intercondylar eminences. Its posteriormost part also faces, in part, posteriorly. On the anterior face of the proximal end is a prominent tibial tuberosity, which slightly curves proximolaterally. The tibial tuberosity leads distally to the tibial crest.

In anterior view, the tibial crest is angled distomedially. It gradually decreases in height distally to become a low ridge. The most salient feature of the distal end is the medial malleolus, which in anterior view forms a near 90° angle with the remaining portion of the tibia's distal edge. In contrast, this angle is obtuse in *Dissacus navajovius* (AMNH 3359) and *Ankalagon saurognathus* (AMNH 776). An elongate fossa is centered on the anterior face of the distal end of the tibia, lateral to the base of the medial malleolus. Lateral to
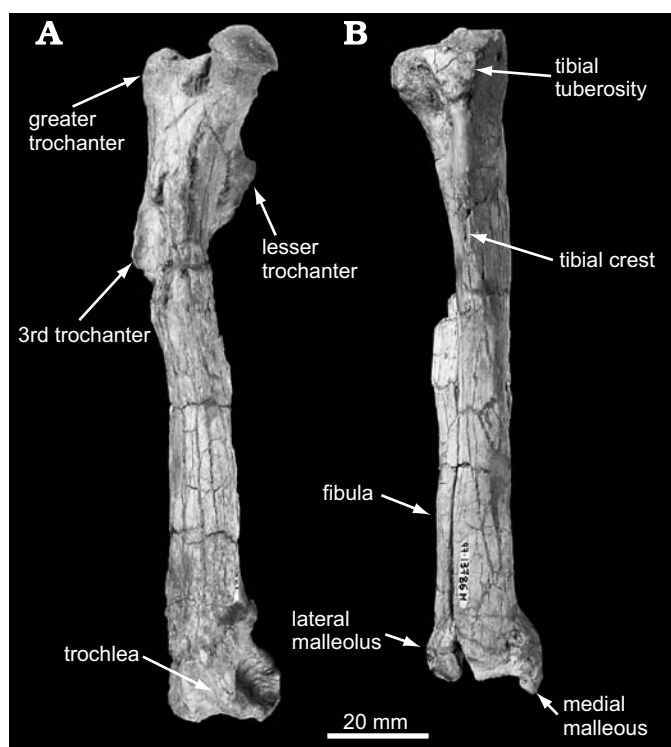

Fig. 9. Anterior views of right femur (**A**) and right tibia and fibula (**B**) of *Dissacus zanabazari* sp. nov., holotype, MAE-BU-97-13786, Tsagaan Khushuu, Gobi Desert, Mongolia, early Eocene.
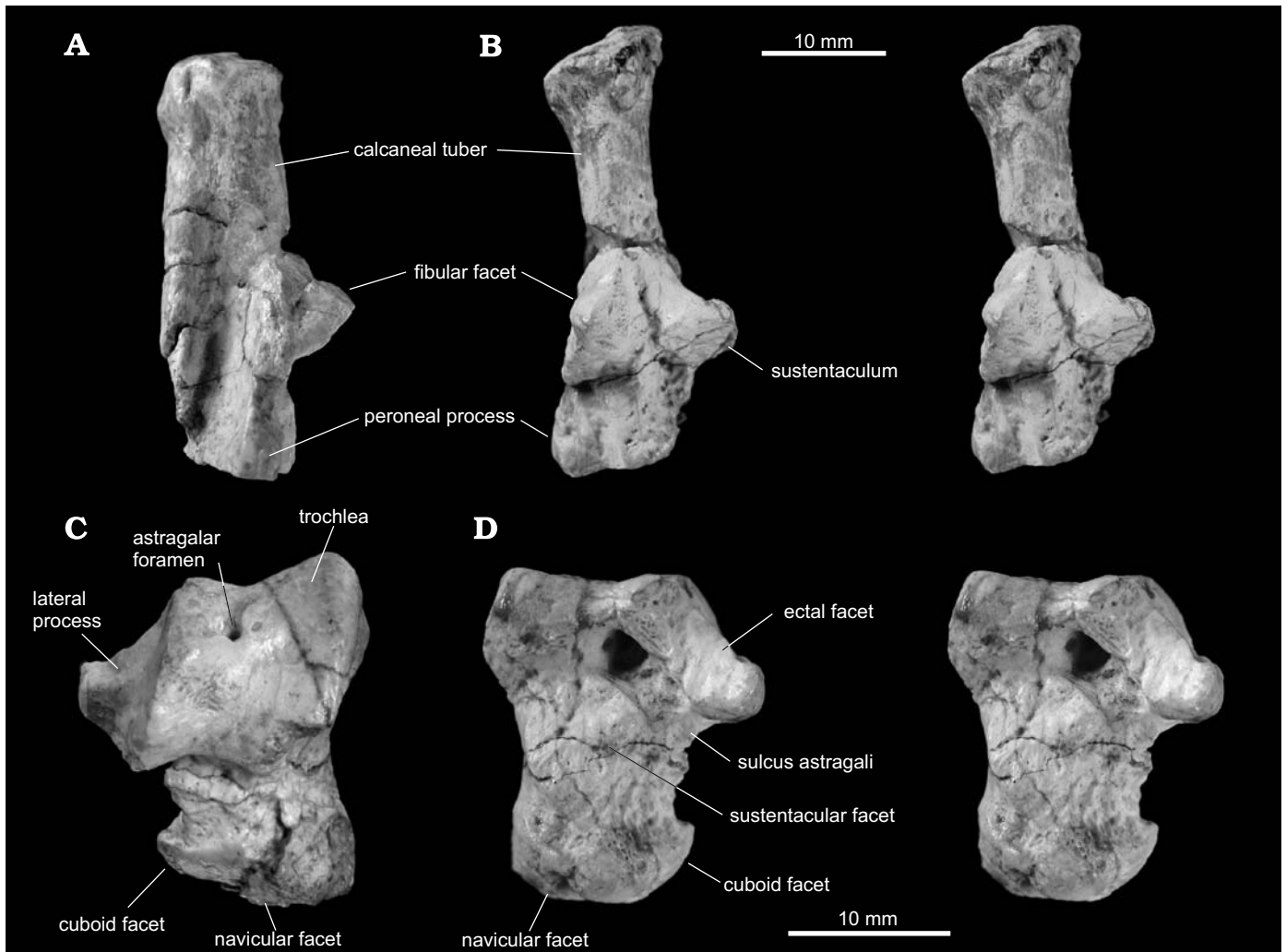
Fig. 10. Proximal tarsal bones of *Dissacus zanabazari* sp. nov., holotype, MAE-BU-97-13786, Tsagaan Khushuu, Gobi Desert, Mongolia, early Eocene. Right calcaneus in lateral view (**A**) and stereopair in anterior view (**B**). Right astragalus in anterodorsal view (**C**) and stereopair in posterior view (**D**).

this fossa is a smooth strip of bone that abutted the astragalus during flexion of the upper tarsal joint.

Fibula.—The distal half of the right fibula was preserved (Fig. 9B). The diaphysis is fairly flat, faces anterolaterally, and is clearly separate from the tibia. At its distal end is the lateral malleolus, which articulated with the astragalus or the calcaneus, depending upon the degree of ankle extension. The lateral side of the medial malleolus bears a median tuberosity, a posterior tuberosity, and an intervening proximodistal groove. The tendons of the extensor digitorum lateralis, fibularis brevis, and peroneus longus probably coursed through this groove. The distal face of the fibula bears three articulating facets: the lateral one articulates with the calcaneus during extension, the middle one articulates with the lateral process of the astragalus during flexion, and the medial one is in continuous contact with the astragalus.

Astragalus.—In the following description, the astragalus is described in digitigrade posture. Proximal and dorsal become near equivalents, as do distal and ventral. The tibial ar-

ticulation surface has two parts: a slightly concave portion on the medial side, and a trochlea bounded by sharp medial and lateral ridges. The trochlea is 10.4 mm wide and 1.4 mm deep. On the astragalar neck is the sharply upturned distal end of the tibial articulation surface, which limits flexion of the pes. In proximal view, the trochlea is not parasagittal but is angled anterolaterally. A small astragalar foramen occurs 1/3 of the distance from the lateral edge of the trochlea (Fig. 10C). The trochlea extends posterior to the astragalar foramen, past the medial side of the latter. The astragalus has a distinct lateral process, which has a calcaneal (ectal) facet on its posterior side and a fibular facet for the lateral malleolus on its lateral side. The distal end of the fibular facet is depressed and limits flexion of the pes.

Extending distomedially from the trochlea is the astragalar neck. In cross-section, the neck is rhomboidal; the lateral side faces partially posterior and the medial side faces partially anterior. The distal end, or head, of the astragalus bears a large articulation facet for the navicular and a much smaller one for the cuboid. The navicular facet is convex

anteroposteriorly, flat to slightly concave transversely, and extends onto the posterior surface. The cuboid facet faces distolaterally.

The most salient feature of the posterior face is a D-shaped sustentacular facet for the calcaneus (Fig. 10D). It nearly contacts the cuboid facet. The ectal facet for the calcaneus is concave, elongate with the long axis distolateral, and faces posterodistally. Separating the sustentacular and ectal facets is a deep astragalar sulcus, which leads into the astragalar canal. In posterior view, a small protuberance is situated distal to the medial trochlear edge. Similar, but larger, protuberances occur in *Ankalagon* (AMNH 777) and *Pachyaena ossifraga* (AMNH 4262). Unlike *Arctocyon* (Russell 1964), the astragalus lacks a groove for the tendon of the flexor digitorum fibulare muscle.

Calcaneus.—Like the astragalus, the calcaneus is oriented as if the animal was digitigrade; distal is towards the calcaneal tuber and proximal is towards the astragalus and cuboid articulation facets. The distal end of the calcaneal tuber is larger than more proximal portions, bears a distomedial protuberance, and lacks medial and lateral processes (Fig. 10B). The tuber's distal face is flattened and bears a small elliptical depression near its ventral margin. As in other mesonychids (O'Leary and Rose 1995b), a deep fossa occupies the entire lateral side of the calcaneus. It is most pronounced towards the proximal end (Fig. 10A).

Projecting from the lateral side of the calcaneus is a medially-facing, convex, and oval surface that articulates with ectal facet of the astragalus. Lateral to it is a small convex articulation surface for the lateral malleolus of the fibula. The most salient feature of the medial side is the sustentaculum tali. Its anterior side bears an oval, concave facet that articulates with the sustentacular facet of the astragalus (Fig. 10B). This surface faces anteriorly, not anterodistally. The two astragalar facets are not aligned; the lateral one is 2 mm closer to the distal end of the tuber. In medial view, the cuboid facet is at a right angle to the long axis of the calcaneal tuber. Adjacent to the medial margin of the cuboid facet is an additional, small, narrow facet for the astragalus. The peroneal tubercle is adjacent to the lateral edge of the cuboid facet.

Distal tarsals.—The proximal side of the navicular articulates with the astragalus, is anteroposteriorly concave, and is transversely flat. On its posterior side is a ventrally hooked plantar process. It rests on the proximal surface of an even larger plantar process of the ectocuneiform. The distal surface of the navicular has a medial facet for the mesocuneiform and a lateral facet for the ectocuneiform, but apparently lacks a facet for the entocuneiform. The mesocuneiform facet is divided by a low ridge into anterior and posterior portions.

The proximal half and the entire anterior side of the cuboid is preserved (Fig. 11). It articulates with the calcaneus on its proximal face. The medial third of the cuboid facet is concave and depressed, and the remaining portion is concave anterolaterally to posteromedially and nearly flat transversely. The
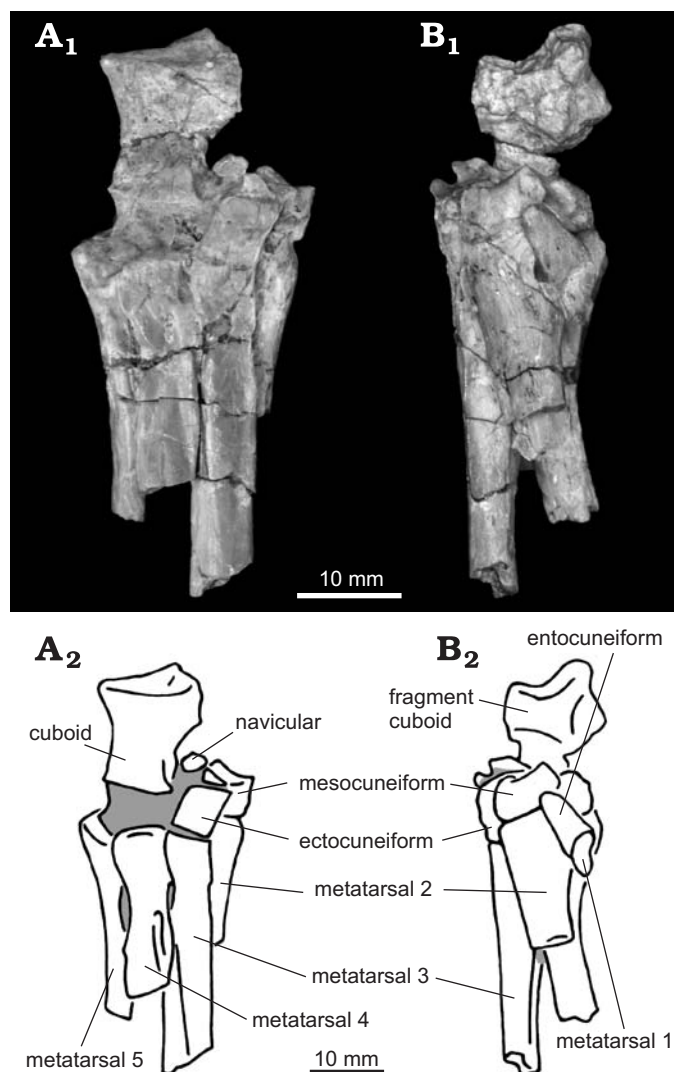

Fig. 11. Partial right tarsus of *Dissacus zanabazari* sp. nov., holotype, MAE-BU-97-13786, Tsagaan Khushuu, Gobi Desert, Mongolia, early Eocene. A_1, anterior view, A_2, explanatory drawing of the same; B_1, medial view, B_2, explanatory drawing of the same.

medial side of the cuboid facet is emarginated by a smaller, highly concave facet for the astragalus. Although the plantar tuberosity is present, its size cannot be determined because of poor preservation.

In anterior view, the ectocuneiform is rhomboidal (i.e., proximal end is more medial than the distal end) and taller than wide (Fig. 11A). The anterior surface is gently convex, the medial surface is concave and articulates with the mesocuneiform, and the lateral surface presumably articulated with the cuboid. The ectocuneiform is elongate anteroposteriorly with a prominent plantar (posterior) process, which has a transversely compressed distal end. The proximal surface of the plantar process has a small concave facet on its anteromedial side for the navicular. The mesocuneiform is much smaller than the ectocuneiform. Its anterior surface is roughly square-shaped and convex with a low median ridge. The proximal face of the mesocuneiform bears a navicular facet, which

is highly concave anteroposteriorly and flat transversely. The entocuneiform is a fairly featureless triangular-shaped bone. Its distal end is concave and articulates with a rudimentary first metatarsal (Fig. 11B).

Metatarsals.—Only the articulated, proximal ends of the metatarsals were preserved. Although their lengths cannot be measured, their widths and positions indicate a paraxonic pes. All metatarsals have flat, not bowed, shafts in lateral view. The 3rd and 4th metatarsals are closely appressed and approximately equal in width (Fig. 11A). Overall the pes is compact with the proximal ends of each metatarsal overlapping its neighbor (e.g., 2nd overlaps the 3rd, 3rd overlaps the 4th,). Only the 3rd and 4th metatarsals have plantar tubercles on their proximal ends. The 3rd's tubercle is much larger than that of the fourth, and its proximal surface is rounded while that of the 4th is concave. Whereas the proximal edges of the 3rd and 4th metatarsals are aligned, the proximal edge of the 2nd metatarsal is about 3.5 mm more proximal. The position of the 2nd metatarsal is unlike the morphology in other mesonychids and may be caused by postmortem disarticulation. The distal end of the 5th metatarsal is curved laterally, indicating that the 5th digit was well separated from the 3rd and 4th digits. The first metatarsal is a small nub of bone triangular in shape with a greatest length of about 6 mm (Fig. 11B). Proximally, the 1st metatarsal articulates with the entocuneiform, the 2nd with the entocuneiform and meso-cuneiform, the 3rd with the ectocuneiform, and the 4th and 5th metatarsals with the cuboid.

Discussion

The phylogenetic analyses of the character matrix (Appendix 3) yielded 8 most parsimonious trees, each 220 steps in length. All most parsimonious trees have a monophyletic Mesonychia, Mesonychidae, and Hapalodectidae. In the strict consensus of the 8 trees (Fig. 12), *Dissacus zanabazari* occurs within Mesonychia, Mesonychidae, and in an unresolved clade with *D. navajovius* and *Ankalagon*. This clade has a Bremer support of one and is diagnosed by the m2 metaconid being subequal to protoconid (character 53, state 2). The absence of the metaconid on m1 is optimized on our most parsimonious trees as being convergent with its loss in more derived mesonychids (e.g., *Mesonyx*, *Pachyaena*). In four of the eight most parsimonious trees, *Dissacus navajovius* and *D. zanabazari* are sister-groups. The sister-group relationship is supported by both taxa sharing a metaconid that is subequal to the protoconid on m1. *Dissacus* is paraphyletic in all most parsimonious trees with *D. navajovius*, *D. zanabazari*, and *D. praenuntius* being more closely related to *Mesonyx*, *Sinonyx* and others than to *D. willwoodensis* and *D. argenteus*. Even though it is beyond the scope of this paper to revise this genus, it seems safe to place the new Mongolian species in *Dissacus* based on its close phylogenetic affinity with the type species, *D. navajovius*.
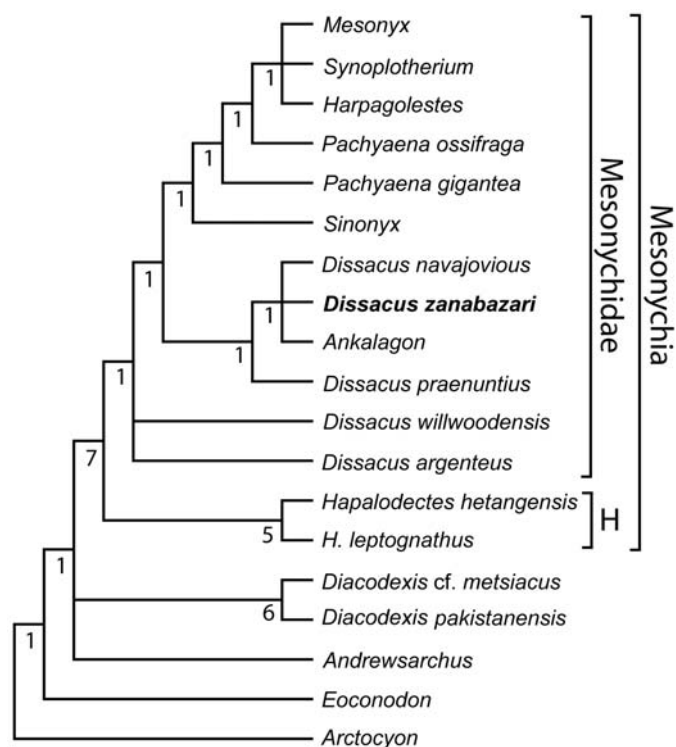

Fig. 12. Phylogenetic position of *Dissacus zanabazari* as depicted in a strict consensus of 8 most parsimonious trees, each 220 steps in length. Bremer support values are placed below and to the left of each node. Abbreviation: H, Hapalodectidae.

Other aspects of our phylogenetic analysis are worthy of note. Mesonychia was strongly supported by a Bremer support of 7. Hapalodectidae has a Bremer support of 5 and is supported by four unequivocal synapomorphies: lower molars very narrow (character 54, state 2), m3 metaconid is a small nub or absent (58, state 2), ectocingula on upper molars (60, state 1), reentrant grooves on proximal sides of lower molars (65, state 0). Support for Mesonychidae is much weaker; it has a Bremer support of 1 and is supported by the following unequivocal synapomorphies: absence of metaconule and hypocone on upper molars (character 62, state 2), reentrant grooves on distal ends of lower molars (65, state 2).

Most of the clades within Mesonychia are weakly supported, with a Bremer support of one. Even with low Bremer support, the clade including *Sinonyx*, *Pachyaena*, *Synoplotherium*, and *Mesonyx* is diagnosed by several characters, including absence of postglenoid foramen (character 1, state 2), narrow gap between occipital condyles (13, state 2 or 3), elongate external auditory meatus (17, state 3), lateral edge of external auditory meatus is bowed dorsally (18, state 1), glenoid fossa far ventral to basicranial stem (19, state 2), highly concave lateral surface of maxilla (31, state 1), apex of lower incisors narrower than base of crown (41, state 0), m1 metaconid is a small nub or absent (48, state 2), and m3 metaconid is a small nub or absent (58, state 2). In trees one step longer than the most parsimonious ones, *Ankalagon* falls

inside this clade, with *Sinonyx* as its basal member. In all most parsimonious trees *Pachyaena* is paraphyletic, with *P. ossifraga* the sister-group to a clade that includes *Mesonyx*, *Synoplotherium*, and *Harpagolestes*. Although both species of *Pachyaena* are unique among mesonychids in having a metaconule on M1 and M2, *P. ossifraga* is more derived than *P. gigantea* in having very elongate external auditory meatus (character 17, state 4) and a m3 with a metacone and metastyle (57, state 0).

The holotype of *Dissacus zanabazari* is the most complete skeleton known of a primitive mesonychid. It provides important new information on the phylogenetic position of Mesonychidae by corroborating observations made in other species as well as by providing details of the anatomy not yet observed in mesonychids. *D. zanabazari* has already been included in three large-scale phylogenetic analyses under the name "Mongolian *Dissacus*" (Geisler 2001; Geisler and Uhen 2003, 2005); therefore, we will primarily focus on the implications of individual features and not synapomorphies as indicated by previous parsimony analyses.

Luo and Gingerich (1999) described the basicranium of *Dissacus praenuntius*. They noted that unlike *Mesonyx*, *D. praenuntius* has a subarcuate fossa. Here we report in *D. zanabazari* the second instance of a subarcuate fossa in mesonychids. Cetaceans also lack a subarcuate fossa; therefore, the presence of the fossa in basal mesonychids is consistent with the view that the loss of the fossa in mesonychids and cetaceans is convergent. *Mesonyx obtusidens* and early cetaceans have a foramen in the vicinity of the petrosal/squamosal suture (Geisler and Luo 1998; Luo and Gingerich 1999). Despite similar positions, Geisler and Luo (1998) suggested that the foramen in cetaceans transmitted the postglenoid vein while the foramen in mesonychids transmitted the superior ramus of the stapedial artery. Their hypothesis is supported by the presence of two foramina in this region in *D. navajovius* (Van Valen 1966) and in *D. zanabazari*, one for the vein and the other for the artery. However unlike *Mesonyx* (Geisler and Luo 1998) and *Dissacus praenuntius* (Luo and Gingerich 1999), the foramen for superior ramus of the stapedial artery in *D. zanabazari* is entirely enclosed in the petrosal, not in the petrosal/squamosal suture.

Owing to the excellent preservation of the holotype, *D. zanabazari* exhibits two features not previously observed in mesonychids. Based on a facet of the entocuneiform, O'Leary and Rose (1995b) inferred that *Pachyaena* had a reduced 1st metatarsal. Their inference is corroborated by the tarsus in the holotype of *D. zanabazari*, which preserves a highly reduced and non-functional 1st metatarsal in articulation with the entocuneiform. A reduced 1st metatarsal also occurs in the primitive artiodactyl *Diacodexis* and in the cetacean *Rodhocetus* (Gingerich et al. 2001), thus reduction of the first metatarsal is a possible synapomorphy of Perissodactyla + Cetartiodactyla + Mesonychia clade. The lower incisors of mesonychids are poorly known, primarily because they typically exhibit heavy wear. The incisors of *D. zanabazari* are less worn, and show that the incisors in this taxon bear three aligned cusps.

Mesonychids are among the better-studied Paleogene groups of mammals, with detailed studies on the dentition (O'Leary and Rose 1995a; O'Leary 1998a), basicranium (Geisler and Luo 1998; Luo and Gingerich 1999), and postcrania (Wortman 1901; O'Leary and Rose 1995b; Rose and O'Leary 1995). Despite these advances, the anatomy of middle Paleocene mesonychids is not well known. Most notable is *Ankalagon*, which is hypothesized to be closely related to *D. navajovius* and *D. zanabazari* (present study) or to be more closely related to *Sinonyx*, *Pachyaena*, *Mesonyx*, and *Harpagolestes* (Zhou et al. 1995; O'Leary 1998a; O'Leary and Geisler 1999). Additional discoveries of Paleocene mesonychids will not only help resolve the phylogeny within the group, but may shed light on the origin of these most peculiar hoofed mammals.

Acknowledgements

References

Asher, R.J., Meng, J., Wible, J.R., McKenna, M.C., Rougier, G.W., Dashzeveg, D., and Novacek, M.J. 2005. Stem Lagomorpha and the antiquity of Glires. *Science* 307: 1091–1094.

Asher, R.J., Novacek, M.J., and Geisler, J.H. 2003. Relationships of endemic African mammals and their fossil relatives based on morphological and molecular evidence. *Journal of Mammalian Evolution* 10: 131–194.

Boisserie, J.-R., Lihoreau, F., and Brunet, M. 2005. The position of Hippopotamidae within Cetartiodactyla. *Proceedings of the National Academy of Sciences* 102: 1537–1541.

Chow, M. 1959. A new arctocyonid from the upper Eocene of Lushih, Honan. *Vertebrata PalAsiatica* 3 (3): 133–138.

Chow, M. and Qi, T. 1978. Paleocene mammalian fossils from Nomogen Formation of Inner Mongolia [in Chinese with English summary]. *Vertebrata PalAsiatica* 16: 77–85.

Chow, M., Zhang, Y., Wang, B., and Ding, S. 1977. Paleocene mammalian fauna from the Nanxiong Basin, Guangdong Province. *Paleontologica Sinica New Series C* 20: 1–100 [in Chinese, with English translation by Will Downs, 2000, Bilby Research Center, Northern Arizona University].

Cifelli, R.L. 1982. The petrosal structure of *Hyopsodus* with respect to that

of some other ungulates, and its phylogenetic implications. *Jounal of Paleontology* 56: 795–805.

Cope, E.D. 1881. Notes on Creodonta. *American Naturalist* 15: 1018–1020.

Dashzeveg, D. 1976. New mesonychids (Condylarthra, Mesonychidae) from the Paleogene of Mongolia [in Russian]. *Sovmestnaâ Soviet-Mongolian Paleontologičeskaâ Ekspediciâ (Trudy)* 3: 14–31.

Dashzeveg, D. 1988. Holarctic correlation of non-marine Paleocene–Eocene boundary strata using mammals. *Journal of the Geological Society, London* 145: 473–478.

Dashzeveg, D., and Russell, D.E. 1988. Paleocene and Eocene Mixodontia (Mammalia, Glires) of Mongolia and China. *Palaeontology* 31: 129–164.

Evans, H.E. 1993. *Miller's Anatomy of the Dog*. 3rd ed. 113 pp. W.B. Saunders Co., Philadelphia.

Gatesy, J. 1997. More DNA support for a Cetacea/Hippopotamidae clade: the blood-clotting protein gamma-fibrinogen. *Molecular Biology and Evolution* 14: 537–543.

Gatesy, J., Hayashi, C., Cronin, A., and Arctander, P. 1996. Evidence from milk casein genes that cetaceans are close relatives of hippopotamid artiodactyls. *Molecular Biology and Evolution* 13: 954–963.

Gatesy, J., Matthee, C., DeSalle, R., and Hayashi, C. 2002. Resolution of the supertree/supermatrix paradox. *Systematic Biology* 51: 652–664.

Geisler, J.H. 2001. New morphological evidence for the phylogeny of Artiodactyla, Cetacea, and Mesonychidae. *American Museum Novitates* 3344: 1–53.

Geisler, J.H. and Luo, Z. 1996. The petrosal and inner ear of *Herpetocetus* sp. (Mammalia: Cetacea) and their implications for the phylogeny and hearing of archaic mysticetes. *Journal of Paleontology* 70: 1045–1066.

Geisler, J.H. and Luo, Z. 1998. Relationships of Cetacea to terrestrial ungulates and the evolution of cranial vasculature in Cete. *In*: J.G.M. Thewissen (ed.), *The Emergence of Whales*, 163–212. Plenum, New York.

Geisler, J.H. and Uhen, M.D. 2003. Morphological support for a close relationship between hippos and whales. *Journal of Vertebrate Paleontology* 23: 991–996.

Geisler, J.H. and Uhen, M.D. 2005. Phylogenetic relationships of extinct cetartiodactyls: results of simultaneous analyses of molecular, morphological, and stratigraphic data. *Journal of Mammalian Evolution* 12 (1 and 2): 145–160.

Gentry, A.W. and Hooker, J.J. 1988. The phylogeny of Artiodactyla. *In*: M.J. Benton (ed.), The Phylogeny and Classification of the Tetrapods, Mammals, Vol. 2. *Systematics Association Special Volume* 35B: 235–272.

Gingerich, P.D., Haq, M.U., Zalmout, I.S., Khan, I.H., and Malakani M.S. 2001. Origin of whales from early artiodactyls: hands and feet of Eocene Protocetidae from Pakistan. *Science* 293: 2239–2242.

Goloboff, P. 1993. *NONA Version 1.9*. Computer Program and Documentation. Available at ftp.unt.edu.ar/pub/parsimony.

Horovitz, I. 2004. Eutherian mammal systematics and the origins of South American ungulates as based on postcranial osteology. *In*: M.R. Dawson and J.A. Lillegraven (eds.), Fanfare for an uncommon paleontologist: papers in honor of Malcolm C. McKenna. *Bulletin of the Carnegie Museum of Natural History* 36: 63–79.

Lemoine, V. 1891. Étude d'ensemble sur les dents des mammifères fossiles des environs de Reims. *Bulletin de la Société Géologique de France* 19: 263–290.

Luckett, W.P. and Hong, N. 1998. Phylogenetic relationships between the orders Artiodactyla and Cetacea: a combined assessment of morphological and molecular evidence. *Journal of Mammalian Evolution* 5: 127–181.

Luo, Z. and Gingerich, P.D. 1999. Terrestrial Mesonychia to aquatic Cetacea: transformation of the basicranium and evolution of hearing in whales. *University of Michigan Papers on Paleontology* 31: 1–98.

Luo, Z. and Marsh, K. 1996. Petrosal (periotic) and inner ear of a Pliocene kogiine whale (Kogiinae, Odontoceti): implications on relationships and hearing evolution of toothed whales. *Journal of Vertebrate Paleontology* 16: 328–348.

MacPhee, R.D.E. 1994. Morphology, adaptations, and relationships of *Plesiorycteropus*, and a diagnosis of a new order of eutherian mammals. *Bulletin of the American Museum of Natural History* 220: 1–214.

Maddison, W.P. and Maddison, D.R. 2000. *MacClade, Vers. 4.0.* Sinauer Associates. Available at http://www.sinauer.com/.

Matthew, W.D. 1897. A revision of the Puerco fauna. *Bulletin of the American Museum of Natural History* 9: 59–110.

Matthew, W.D. 1937. Paleocene faunas of the San Juan Basin, New Mexico. *Transactions of the American Philosophical Society* 30: 1–510.

Matthee, C.A., Burzlaff, J.D., Taylor, J.F., and Davis, S.K. 2001. Mining the mammalian genome for artiodactyl systematics. *Systematic Biology* 50: 367–390.

McKenna, M.C. and Bell, S.K. 1997. *Classification of Mammals above the Species Level*. 631 pp. Columbia University Press, New York.

Meng, J. and McKenna, M.C. 1998. Faunal turnovers of Paleogene mammals from the Mongolian Plateau. *Nature* 394: 364–367.

Meng, J., Zhai, R., and Wyss, A.R. 1998. The late Paleocene Bayan Ulan fauna of Inner Mongolia. *In*: K.C. Beard and M.R. Dawson (eds.), Dawn of the age of mammals in Asia. *Bulletin of the Carnegie Museum of Natural History* 34: 148–185.

Nixon, K.C. 1999. The parsimony ratchet, a new method for rapid parsimony analysis. *Cladistics* 15: 407–414.

Novacek, M.J. 1986. The skull of lepticitid insectivorans and the higher-level classification of eutherian mammals. *Bulletin of the American Museum of Natural History* 183: 1–112.

O'Leary, M.A. 1998a. Phylogenetic and morphometric reassessment of the dental evidence for a mesonychian and cetacean clade. *In*: J.G.M. Thewissen (ed.), *The Emergence of Whales*, 133–161. Plenum Press, New York.

O'Leary, M.A. 1998b. Morphology of the humerus of *Hapalodectes* (Mammalia, Mesonychia). *American Museum Novitates* 3242: 1–6.

O'Leary, M.A. and Geisler, J.H. 1999. The position of Cetacea within Mammalia: Phylogenetic analysis of morphological data from extinct and extant taxa. *Systematic Biology* 48: 455–490.

O'Leary, M.A. and Rose, K.D. 1995a. New mesonychian dentitions from the Paleocene of the Bighorn Basin, Wyoming. *Annals of Carnegie Museum* 64: 147–172.

O'Leary, M.A., and Rose, K. D. 1995b. Postcranial skeleton of the Early Eocene mesonychid *Pachyaena* (Mammalia: Mesonychia). *Journal of Vertebrate Paleontology* 15: 401–430.

O'Leary, M.A., Lucas, S.G., and Williamson, T.E. 2000. A new specimen of *Ankalagon* (Mammalia, Mesonychia) and evidence of sexual dimorphism in mesonychians. *Journal of Vertebrate Paleontology* 20: 387–393.

Rose, K.D. 1985. Comparative osteology of North American dichobunid artiodactyls. *Journal of Paleontology* 59: 1203–1226.

Rose, K.D. and O'Leary, M.A. 1995. The manus of *Pachyaena gigantea* (Mammalia: Mesonychia). *Journal of Vertebrate Paleontology* 15: 855–859.

Russell, D.E. 1964. Les mammifères Paléocènes d'Europe. *Memoires du Museum national d'Histoire naturelle, Serie C – Sciences de la Terre* 13: 1–324.

Russell, D.E., Thewissen, J.G.M., and Sigogneau-Russell, D. 1983. A new dichobunid artiodactyl (Mammalia) from the Eocene of North-West Pakistan, Part II: Cranial osteology. *Proceedings of the Koninklijke Nederlandse Akademie van Weenschappen B* 86: 285–299.

Schaeffer, B. 1947. Notes on the origin of the artiodactyl tarsus. *American Museum Novitates* 1356: 1–24.

Scott, W.B. 1888. On some new and little known creodonts. *Journal of the Academy of Natural Sciences Philadelphia* 9: 155–185.

Shimamura, M., Yasue, H., Ohshima, K., Abe, H., Kato, H., Kishiro, T., Goto, M., Munechika, I., and Okada, N. 1997. Molecular evidence from retroposons that whales form a clade within even-toed ungulates. *Nature* 388: 666–670.

Shoshani, J. 1986. Mammalian phylogeny: comparison of morphological and molecular results. *Molecular Biology and Evolution* 3: 222–242.

Sorenson, M.D. 1996. *TreeRot*. University of Michigan, Ann Arbor. Available at http://people.bu.edu/msoren/TreeRot.html.

Swofford, D.L. 2002. *PAUP*, Phylogenetic Analysis Using Parsimony*

(*and other methods*). Sinauer Associates. Vers. 4.0b10. Available at http://paup.csit.fsu.edu/.

Szalay, F.S. 1969. Origin and evolution of function of the mesonychid condylarth feeding mechanism. *Evolution* 23: 703–720.

Theodor, J.M. and Foss, S.E. 2005. Deciduous dentitions of Eocene cebochoerid artiodactyls and cetartiodactyl relationships. *Journal of Mammalian Evolution* 12 (1 and 2): 161–181.

Thewissen, J.G.M. 1994. Phylogenetic aspects of cetacean origins: A morphological perspective. *Journal of Mammalian Evolution* 2: 157–183.

Thewissen, J.G.M. and Domning, D.P. 1992. The role of phenacodontids in the origin of the modern orders of ungulate mammals. *Journal of Vertebrate Paleontology* 12: 494–504.

Thewissen, J.G.M. and Hussain, S.T. 1990. Postcranial osteology of the most primitive artiodactyl *Diacodexis pakistanensis* (Dichobunidae). *Anatomia, Histologia, Embryologia* 19: 37–48.

Thewissen, J.G.M. and Madar, S.I. 1999. Ankle morphology of the earliest cetaceans and its implications for the phylogenetic relations among ungulates. *Systematic Biology* 48: 21–30.

Thewissen, J.G.M., Russell, D.E., Gingerich, P.D., and Hussain, S.T. 1983. A new dichobunid artiodactyl (Mammalia) from the Eocene of North-West Pakistan, Dentition and Classification. *Proceedings of the Koninklijke Nederlandse Akademie van Weenschappen B* 86: 153–180.

Thewissen, J.G.M., Williams, E.M., Roe, L.J., and Hussain, S.T. 2001. Skeletons of terrestrial cetaceans and the relationship of whales to artiodactyls. *Nature* 413: 277–281.

Ting, S. and Li, C. 1987. The skull of *Hapalodectes* (?Acreodi, Mammalia), with notes on some Chinese Paleocene mesonychids. *Vertebrata PalAsiatica* 25: 161–186.

Ting., S., Wang, Y., Schiebout, J.A., Koch, P.L., Clyde, W.C., Bowen, G.J., and Wang, Y. 2004. New early Eocene mammalian fossils from the Hengyang Basin, Hunan China. *In*: M.R. Dawson and J.A. Lillegraven (eds.), Fanfare for an uncommon paleontologist: papers in honor of Malcolm C. McKenna. *Bulletin of the Carnegie Museum of Natural History* 36: 291–301.

Tong, Y. and Wang, J. 1988. A preliminary report on the early Eocene mammals of the Wutu fauna, Shandong Province, China. *In*: K.C. Beard and M.R. Dawson (eds.), Dawn of the Age of Mammals in Asia. *Bulletin of the Carnegie Museum of Natural History* 34: 186–193.

Van Valen, L. 1966. Deltatheridia, a new order of mammals. *Bulletin of the American Museum of Natural History* 132: 1–126.

Wang, B.Y. 1975. Paleocene mammals of Chaling Basin, Hunan [in Chinese]. *Vertebrata PalAsiatica* 13: 154–164.

Webb, S.D. and Taylor, B.E. 1980. The phylogeny of hornless ruminants and a description of the cranium of *Archaeomeryx*. *Bulletin of the American Museum of Naural History* 167: 121–157.

Wible, J.R. 1990. Petrosals of Late Cretaceous marsupials from North America, and a cladistic analysis of the petrosal in therian mammals. *Journal of Vertebrate Paleontology* 10: 183–205.

Wilkinson, M. 1992. Ordered *versus* unordered characters. *Cladistics* 8: 375–385.

Wortman, J.L. 1901. Studies of the Eocene Mammalia in the Marsh collection, Peabody Museum. *American Journal of Science* 11: 1–90.

Yan, D.F. and Tang, Y.J. 1976. Mesonychids from the Paleocene of Anhui [in Chinese]. *Vertebrata PalAsiatica* 14: 252–258.

Zhou, X., Zhai, R., Gingerich, P.D., and Chen, L. 1995. Skull of a new mesonychid (Mammalia, Mesonychia) from the Late Paleocene of China. *Journal of Vertebrate Paleontology* 15: 387–400.

Appendix 1

Specimens examined and references consulted for diagnosis and phylogenetic analysis.

Andrewsarchus: AMNH 20135; Chow (1959).

Ankalagon saurognathus: AMNH 776, 777, 2454; O'Leary et al. (2000).

Arctocyon: AMNH 55900 (cast), 55901 (cast), 55902; Russell (1964).

Diacodexis cf. *metsiacus*: AMNH 4700, 16141, 128563 (cast); Rose (1985).

Diacodexis pakistanensis: Russell et al. (1983); Thewissen et al. (1983); Thewissen and Hussain (1990).

Dissacus argenteus: AMNH 131916 (cast of YPM-PU 16135); O'Leary and Rose (1995a).

Dissacus indigenus: Dashzeveg (1976).

Dissacus magushanensis: AMNH 122014 (cast of IVPP V4266); Yan and Tang (1976).

Dissacus navajovius: AMNH 3356, 3359, 3360, 3361, 15996.

Dissacus praenuntius: AMNH 16069, 131913 (cast of YPM-PU 13295), 131917 (cast of YPM-PU 19597); O'Leary and Rose (1995a); Luo and Gingerich (1999).

Dissacus rotundus: AMNH 122013 (cast of IVPP V4868.4); Wang (1975).

Dissacus serratus: Chow and Qi (1978); Meng et al. (1998).

Dissacus willwoodensis: AMNH 131915 (cast of YPM-PU 16137), 131920 (cast of USGS 27635); O'Leary and Rose (1995a).

Dissacus zanabazari: MAE-BU97-13786.

Dissacus zengi: Ting et al. (2004).

Eoconodon: AMNH 764, 774, 3177, 3181, 3187, 3280, 4052, 16329, 16341; Matthew (1897, 1937).

Hapalodectes hetangensis: IVPP V5253; Ting and Li (1987).

Hapalodectes leptognathus: AMNH 78, 12781, 128561, 14748 (cast); IVPP V5253; Szalay (1969); O'Leary (1998b).

Harpagolestes: AMNH 1692, 1878, 1892, 1945, 2302, 2308, 26267, 26300, 26301; Wortman (1901); Zhou et al. (1995).

Mesonyx obtusidens: AMNH 11552, 12643, 93451; Scott (1888).

Pachyaena gigantea: AMNH 72, 2959, 15226, 15227; O'Leary and Rose (1995b); Rose and O'Leary (1995).

Pachyaena ossifraga: AMNH 75, 4262, 4263, 15222, 15224, 15730, 16154; O'Leary and Rose (1995b).

Sinonyx jiashanensis: IVPP V10760; Zhou et al. (1995).

Synoplotherium lanius: AMNH 19203; Wortman (1901).

Yantanglestes feiganensis: Chow et al. (1977).

Appendix 2

Morphological character descriptions

This appendix defines the 89 morphological characters used in the cladistic analysis. Unqualified citations indicate that the character is worded with little or no modification from the given reference. Multiple citations indicate more detailed descriptions, additional character states, illustrations, or other improvements of a character, as compared to its first use. Most of the characters come directly from Geisler (2001), and the number of a character in that reference is abbreviated G#. Geisler (2001) also includes quantitative descriptions for some of the qualitative character states used here.

1. *Size of postglenoid foramen* (ordered). Large (0); similar in size to fenestra vestibuli (1); absent (2) (Geisler and Luo 1998; O'Leary and Geisler 1999; G07).
2. *Posttemporal canal (for arteria diploetica magna, also called percranial foramen).* Present (0); absent (1) (Wible 1990; MacPhee 1994; G10).
3. *Epitympanic sinus in squamosal.* Present, situated in anterolateral corner of the roof of the middle ear (0); absent (1).
4. *Shape of tegmen tympani.* Forms lamina lateral to facial nerve canal (0); inflated (1) (Cifelli 1982; Geisler and Luo 1998; Luo and Gingerich 1999; O'Leary and Geisler 1999; G12).
5. *Fossa for tensor tympani muscle.* Shallow anteroposteriorly elongate fossa (0); circular pit (1) (Geisler and Luo 1998; Luo and Gingerich 1999; G14).
6. *Perilymphatic foramen.* Situated in wide fossa (0); not in a fossa (1).
7. *Articulation of pars cochlearis with basisphenoid/basioccipital.* Present (0); absent (1) (Thewissen and Domning 1992; G16).
8. *Ectotympanic part of the meatal tube* (ordered). Absent (0); present but short (1); present and long (2) (Geisler and Luo 1998; G28).
9. *Posterior edge of squamosal.* Flat (0); sharply upturned (1); sharply upturned and bears dorsally projecting process (2) (Gentry and Hooker 1988; G31).
10. *Sagittal crest* (ordered). Absent or barely present (0); small (1); substantial (2); dorsally expanded, (3) (G33).
11. *Dorsal edge of braincase, relative to occlusal plane.* Slopes posterodorsally (0); approximately level (1); curves posteroventrally (2) (G34).
12. *Foramen magnum* (ordered). Large, maximum dorsoventral diameter > 28% the basicranial width at the level of the external auditory meatus (0); intermediate, 24% > foramen magnum height > 15% the basicranial width (1); small, foramen magnum height < 14% the basicranial width (2).
13. *Separation between occipital condyles* (ordered). Very large, ventral gap between condyle > 74% of maximum basioccipital width (0); large, 64% > condylar gap > 55% basioccipital width (1); moderate separation, 50% > condylar gap > 30% (2); narrow, gap < 25% basioccipital width (3).
14. *Facial nerve sulcus distal to stylomastoid foramen.* Absent (0); anterior wall of sulcus formed by squamosal (1); anterior wall formed by mastoid process of petrosal (2); anterior wall formed by meatal tube of ectotympanic (3) (Geisler and Luo 1998; O'Leary and Geisler 1999; G35).
15. *Length of mastoid process of petrosal* (ordered). Ventral portion absent (0); ventral portion short (1); elongate, (2); hypertro-

phied, (3) (Geisler and Luo 1996; Luo and Marsh 1996; Geisler and Luo 1998; G36).
16. *Angle of suture of squamosal with petrosal or exoccipital, skull in ventral view* (ordered). Forms a 147° angle with the sagittal plane (0); forms an angle between 127° and 125° (1); angle between 111° and 105° (2), angle <100° (3) (G39).
17. *Length of external auditory meatus of the squamosal* (ordered). Absent (0); very short, transverse "length" of meatus < 12% the basicranial width at the level of the meatus(1); intermediate, 15% < meatus length < 20% basicranial width (2); long, 20% < meatus length < 23% (3); very long, meatus length > 26% of basicranial width (similar to G40).
18. *Edge of external auditory meatus.* With skull in lateral view, the dorsal edge is nearly flat (0); edge is bowed dorsally (1).
19. *Glenoid fossa* (ordered). In same plane as basisphenoid and basioccipital (0); slightly ventral to these bones (1); far ventral to these bones (2).
20. *Preglenoid process.* Absent (0); present (1) (Thewissen 1994; Geisler and Luo 1998; G44).
21. *Foramen ovale.* Anterior to glenoid fossa (0); medial to glenoid fossa (1) (Zhou et al. 1995; Geisler and Luo 1998; G45).
22. *Zygomatic portion of jugal.* Directed posterolaterally (0); directed posteriorly (1) (G48).
23. *Alisphenoid canal (alar canal).* Present (0); absent (1) (Novacek 1986; Thewissen and Domning 1992; G49).
24. *Contact of frontal and maxilla in orbit.* Absent (0); present (1) (Novacek 1986; Thewissen and Domning 1992; G52).
25. *Postorbital process of jugal* (ordered). Absent (0); present but does not contact frontal (1); with frontal forms a postorbital bar (2) (Gentry and Hooker 1988; G55).
26. *Ventral edge of orbit.* Projects dorsally (0); flared laterally (1) (G56).
27. *Position of orbit relative to toothrow* (ordered). Over P4 or P4/M1 division (0); over M1 or M1/M2 division (1); over M2 or M2/M3 division (2); over or posterior to M3 (3) (G57).
28. *Lacrimal foramina.* Two (0); one (1) (Gentry and Hooker 1988; G59).
29. *Elongation of face* (ordered). Face short (0); intermediate in length (1); long (2) (G64).
30. *Anterior opening of infraorbital canal.* Over M1 or P4 (0); at level between P3 and P4 (1) (G65).
31. *Lateral surface of maxilla.* Flat or slightly concave (0); highly concave (1) (G66).
32. *Posterior edge of nasals.* Terminate anterior to orbit (0); terminate posterior to the anterior edge of the orbit (1) (G67).
33. *Palate.* Flat (0); vaulted (1) (G69).
34. *Embrasure pits on palate.* Absent (0); present (1) (Thewissen 1994; Geisler and Luo 1998; G70).
35. *Angular process of mandible.* No dorsal hook (0); dorsal hook present (1) (Gentry and Hooker 1988; G72).
36. *Medial inflection of mandibular angle.* Absent (0); present (1) (Szalay 1969).
37. *Height of coronoid process* (ordered). Low (0); high (1); very high (2) (G76).
38. *Deep concavity on lateral surface of mandible between condyle and coronoid process if dentary.* Absent (0); present (1) (Gentry and Hooker 1988; G77).
39. *Ramus of mandible.* Approximately same dorsoventral thick-

ness from m1 to m3 (0); deepens posteriorly from m1 to m3 (1) (Gentry and Hooker 1988; G79).

40. *Number of lower incisors* (ordered). Three (0); two (1); one (2).

41. *Lower incisors*. Apex of cusp pointed or narrower than base (0); spatulate (1); peg-shaped (2); tusk-like (3) (G83).

42. *P1*. Absent (0); present, one-rooted (1) (Zhou et al. 1995; O'Leary 1998a; G88).

43. *P3 roots*. Three (0); two (1) (Zhou et al. 1995; G91).

44. *P4 metacone*. Absent (0); present (1) (G95).

45. *P4 entocingulum*. Present (0); absent or very small (1) (G96).

46. *Stylar shelves*. Present, occurs on anterolateral and posterolateral corners of molars (0); absent (1).

47. *M1 parastyle* (ordered). Absent (0); weak (1); moderate to strong (2) (Zhou et al. 1995; O'Leary 1998a; G99).

48. *m1 metaconid* (ordered). Subequal to protoconid (0); smaller than protoconid (1); forms a lingual swelling on protoconid or absent (2).

49. *Postprotocristid on m1 and m2* (ordered). Absent (0); present, connects protoconid to cristid obliqua (1); present and forms a carnassial notch with cristid obliqua (2).

50. *Labial edge of lower molars*. With tooth in occlusal view, edge emarginated between protoconid and hypoconid (0); edge is straight (1).

51. *Protoconid* (ordered). Anterolateral to metaconid (0); in transverse line with metaconid (1); posterolateral to metaconid (2).

52. *M2 metacone* (ordered). Subequal to paracone (0); approximately half the size of the paracone (1); highly reduced, indistinct from paracone (2) (Zhou et al. 1995; O'Leary 1998a; G101).

53. *m2 metaconid* (ordered). Subequal to protoconid (0); smaller than protoconid (1); forms a lingual swelling on protoconid or absent (2).

54. *m2 width* (ordered). Wide, maximum width > 60% the maximum length (0); intermediate width, 60% > width > 34% length (1); very narrow, width < 34% the maximum length.

55. *M3* (ordered). Larger than M2 (0); approximately equal to M2 (1); reduced, maximum mesodistal length <60% the length of M2 (2); absent (3) (Zhou et al. 1995; Geisler and Luo 1998; G103).

56. *m3 hypoconulid*. Protrudes as separate distal lobe (0); absent (2) (Thewissen 1994; G105).

57. *Number of labial cusps on M3*. Three cusps (0); two cusps, metacone or metastyle missing (1).

58. *m1 metaconid* (ordered). Subequal to protoconid (0); smaller than protoconid (1); forms a lingual swelling on protoconid or absent (2).

59. *Postprotocristid on m3* (ordered). Absent (0); present, connects protoconid to cristid obliqua (1); present and forms a carnassial notch with cristid obliqua (2).

60. *Ectocingula on upper molars*. Present (0); absent (1) (O'Leary 1998a; G108).

61. *Paraconule of upper molars* (ordered). Present (0); reduced (1); absent (2) (O'Leary 1998a; G110).

62. *Number of cusps in posterolingual quadrant of M1 and M2*. Two, both hypocone and metaconule present (0); one, hypocone or metaconule present (1); none (2) (G111).

63. *Lower molar paraconid or paracristid position*. Cusp lingual or crest winds lingually (0); cusp anterior or crest straight mesodistally on lingual margin (1) (O'Leary 1998a; G115).

64. *Molar protoconid*. Subequal to height of talonid (0); closer to twice height of talonid or greater (1) (O'Leary 1998a; G120).

65. *Reentrant grooves* (ordered). Proximal (0); absent (1); distal (2) (Thewissen 1994; O'Leary 1998a; G122).

66. *Talonid basins*. Broad (0); compressed (1) (Zhou et al. 1995; O'Leary and Rose 1995a; Geisler and Luo 1998; G123).

67. *Occipital condyles*. Broadly rounded in lateral view (0); V-shaped in lateral view, in posterior view the condyle is divided into a dorsal and a ventral half by a transverse ridge (1) (G124).

68. *Atlantoid facet of axis vertebra*. Restricted in coverage (0); extended dorsally at least halfway up neural arch (1) (Webb and Taylor 1980; G127).

69. *Entepicondyle of humerus*. Wide (0); narrow (1) (O'Leary and Rose 1995b; Geisler and Luo 1998; G134).

70. *Length of olecranon process*. Short (0); long (1) (O'Leary and Rose 1995b; O'Leary and Geisler 1999; G138).

71. *Centrale* (ordered). Present and large (0); present but small (1); absent (2) (Thewissen 1994; G143).

72. *Manus*. Mesaxonic (0); paraxonic (1) (O'Leary and Geisler 1999; G145).

73. *Proximal halves of 3rd and 4th metacarpals*. Separate (0); contact each other (1).

74. *Width of middle portion of second metacarpal*. Wide (0); constricted (1) (G148).

75. *Proximal end of 5th metacarpal*. Expanded laterally (0); in line with shaft, not expanded (1).

76. *Greater trochanter of femur* (ordered). Below level of head of femur (0); approximately same level as head of femur (1); elevated dorsally well beyond head of femur (2) (O'Leary and Rose 1995b; G151).

77. *Third trochanter of femur*. Present (0); highly reduced (1) (Luckett and Hong 1998; O'Leary and Geisler 1999; G152).

78. *Proximal end of astragalus* (ordered). Nearly flat to slightly concave (0); well grooved (1); deeply grooved (2) (derived from Schaeffer 1947; O'Leary and Geisler 199; G156).

79. *Astragalar canal*. Present (0); absent (1) (Shoshani 1986; G157).

80. *Navicular facet of astragalus* (ordered). Convex (0); saddle-shaped (1) (Schaeffer 1947; Thewissen and Domning 1992; Geisler and Luo 1998; G158).

81. *Distal end of astragalus contacts cuboid*. contact present but small (0); contact large, facet almost forms a right angle with the parasagittal plane (2) (G159).

82. *Lateral process of astragalus*. Present, ectal facet of the astragalus faces in the plantar direction and its distal end points laterally (0); absent, ectal facet faces laterally and its long axis is parasagittal (1) (Schaeffer 1947; G162).

83. *Sustentacular facet of calcaneus*. Open, facet primarily faces to main body of astragalus (0); faces primarily to astragalar/navicular joint.

84. *Ridge on plantar surface of calcaneus*. Absent or poorly developed (0); present and well defined, helps define a fossa on the lateral surface of the calcaneus (1).

85. *Lateral astragalar facet on calcaneus*. Not in transverse line with sustentacular facet, instead closer to tip of calcaneal tuber (0); nearly aligned with sustentacular facet (1).

86. *Width of the middle portion of the second metatarsal* (ordered). Wide (0); constricted (1); highly compressed (2) (G172).

87. *Elongation of third metatarsal* (ordered). Absent (0); slight elongation (1); substantial elongation (2) (G175).

88. *Ventral edge of distal phalanges of foot*. Distinctly concave (0); flat (1) (O'Leary and Geisler 1999; G179).

89. *Distal phalanges of foot in dorsal view*. Phalanx compressed transversely (0); broad transversely, each phalanx is bilateral with central anteroposterior axis (1); broad transversely, each phalanx is asymmetrical (2) (O'Leary and Geisler 1999; G180).

Appendix 3

Character/taxon matrix.

Explanations: A = 0 + 1, B = 1 + 2, C = 0 + 3, D = 2 + 3, E = 1 + 2 + 3.

```
                             10         20         30         40         50
Arctocyon                1010000?13 0??C111011 11?0001121 011000?100 ?000010010
Diacodexis pakistanensis 010?1??A?1 100?012000 11011?2101 ?0?0102100 1100111000
Diacodexis metsiacus     010?1?1??? ?1?200100? ??0??????1 ?110???10? 1?00111000
Eoconodon                00101?1?12 121C122011 001?002?00 0110101?02 ?000010070
                                                                        
Andrewsarchus            0????????2 A20?234?21 101?113?11 0?10???10? ?00?010???
Hapalodectes hetangensis 000?0?0?00 1??C000?01 1011210101 00010?1?0? ?001?12121
Hapalodectes leptognathus ?????????? ?????????? ?????D??1 ??01???10? ????01??21
Dissacus praenuntius     B0?1?1???? ???2132??1 0????????? ????0?1?0? ???1??2121
Dissacus navajovius      1??1?????? ??????D??1 00??0011?1 ??01???10? ??01002021
Dissacus argenteus       ?????????? ?????????? ?????????? ????????0? ?????02121
Dissacus willwoodensis   ?????????? ?????????? ?????????? ????????1? ???00?2121
Ankalagon                1?0??????? ?????????1 0????????? ????000101 ??01?02221
Dissacus zanabazari      100?111?0? ?01?A22011 0?1??011?1 0101??E100 1001002021
Sinonyx                  20??1?0213 0131123121 ??10002001 11000?1000 000A002221
Pachyaena gigantea       ?0?????20D 0???23D1B1 0???0?20A1 1?1001000? ?A11002221
Pachyaena ossifraga      ?0?1????1D ???2B34121 001?A02101 1110011101 ?011002221
Mesonyx                  2011101213 1121134121 001?0?2101 ?11001?111 00A1012221
Synoplotherium           20?????213 113?134121 001?002100 ?110010102 ?????12B21
Harpagolestes            ?0?????213 0121134121 101?102110 111A010001 ?011012?21


                             60         70         80         89
Arctocyon                1000200010 0000100?00 2???000010 000002001
Diacodexis pakistanensis 1000100000 0100101A?0 20011B1202 11??1?100
Diacodexis metsiacus     1000100000 010010111? ?????11202 111111210
Eoconodon                0000200000 1000?0??0? ???????11? ?0?00????
Andrewsarchus            ?0??000?20 01?0A00??? ?????????? ?????????
Hapalodectes hetangensis 1112?1?221 211101???? ?????????? ?????????
Hapalodectes leptognathus 2112210221 211101???? ?????????? ?????????
Dissacus praenuntius     2111211120 221121???? ?????????? ???1?????
Dissacus navajovius      11A1211120 221121000? ???????111 00011????
Dissacus argenteus       2?11?10111 221121???? ?????????? ?????????
Dissacus willwoodensis   2?11210120 221121???? ?????????? ?????????
Ankalagon                21012111B0 221121?00? 00000A0111 00011????
Dissacus zanabazari      21012110?0 221121000? 0110110111 001110???
Sinonyx                  ??112112B0 2211210??? ?????????? ?????????
Pachyaena gigantea       21212112B0 2111210011 11000??112 00?11??11
Pachyaena ossifraga      2121210220 2111210011 1100020112 001110011
Mesonyx                  ?12131?221 2211210111 0111110102 001110?11
Synoplotherium           2121210??1 ?B1121??11 1100110?02 00???0011
Harpagolestes            ?2B031?B11 2211210?11 A?1?0?0??? ?????????
```